Ion Channel Reconstitution Platform Allowing Simultaneous Recording from Multiple Bilayer Sites

by

Shankar Ramakrishnan

A Thesis Presented in Partial Fulfillment
of the Requirements for the Degree
Master of Science

Approved April 2011 by the
Graduate Supervisory Committee:

Michael Goryll, Chair
Jennifer Blain Christen
Trevor Thornton

ARIZONA STATE UNIVERSITY

May 2011

ABSTRACT

The purpose of this study is to demonstrate that stable lipid bilayers can be set up on an array of silicon micropores and can be used as sites for self-inserting ion-channel proteins which can be studied independently of each other.

In course of this study an acrylic based holder was designed and machined to ensure leak-free fluidic access to the silicon micropores and physical isolation of the individual array channels. To measure the ion-channel currents, we simulated, designed and manufactured low-noise transimpedance amplifiers and support circuits based on published patch clamp amplifier designs, using currently available surface-mount components. This was done in order to achieve a reduction in size and costs as well as isolation of individual channels without the need for multiplexing of the input.

During the experiments performed, stable bilayers were formed across an array of four vertically mounted 30 µm silicon micropores and OmpF porins were added for self insertion in each of the bilayers.

To further demonstrate the independence of these bilayer recording sites, the antibiotic Ampicillin (2.5 mM) was added to one of the fluidic wells. The ionic current in each of the wells was recorded simultaneously. Sub-conductance states of Ompf porin were observed in two of the measurement sites. In addition, the conductance steps in the site containing the antibiotic could be clearly seen to be larger compared to those of the unmodified site. This is due to the transient blocking of ion flow through the porin due to translocation of the antibiotic.

Based on this demonstration, ion-channel array reconstitution is a potential method for efficient electrophysiological characterization of different types of ion-channels simultaneously as well as for studying membrane permeation processes.

To

My Family and Teachers

ACKNOWLEDGMENTS

I would like to take this opportunity to thank all the people who have contributed to my work and supported me in making this thesis a reality.

Firstly, I offer my sincere gratitude to my graduate advisor Dr. Michael Goryll, for accepting me as his Masters' student and giving me a chance to work under his guidance. His patience in dealing with my many questions and mistakes in innumerable situations has helped me to better understand the work that I am dealing with. He has been equally involved in all the experiments that we performed and this strengthened my confidence at times when I worked alone at the laboratory. He is an inspiration that pushes me to put in my best effort in whatever I do in this field and outside of it. Our interaction with each other for extended hours, both in the laboratory, or his office or over coffee has resulted in a fantastic working relationship which I am sure will continue in the future.

I also would like to thank Dr. Trevor Thornton, although I did not have a chance to interact with him during weekly group meetings. My Masters' experience in the United States started with Dr. Thornton's class on the first day, which was crucial for the rest of my coursework and opinion about it. Taking his microelectronics course was a great experience and was instrumental in choosing the research work that I did. I am grateful to him for accepting to be a member of my committee.

I would also like to thank my lab partner and good friend Xiaofeng for the loads of coffee breaks that we took together, PJ for his challenging questions that

made me think and Yunze, for support during the three months of his work in the laboratory.

My sincere thanks goes to my supervisor at the Chemistry stockroom at ASU, Melinda Schermerhorn, who is a wonderful person to have for a boss and Lane Briley, building manager, Physical Sciences who made it possible for me to access tools and get things done as fast as possible. Their support was invaluable for completion of work on time. In addition I would like to mention every person with the ASU machine shop whose advice and ideas helped me design the multi–well acrylic holder.

Above all these wonderful people, I thank my roommates for their support and putting up with my random schedules. My acknowledgement would be incomplete without mentioning the loving and caring family at Arizona in the form of The Faithful City at Tempe and all my mentors and friends here. Their support and advice has been instrumental in the successful completion of my work. No words can express my heartfelt gratitude to my parents and sister in India for their support and in listening to me over phone about cells and lipids. Without their support and belief in me none of this would have been ever possible.

TABLE OF CONTENTS

Page

LIST OF TABLES

Table Page

LIST OF FIGURES

Figure Page

Figure Page

Chapter 1

INTRODUCTION

1.1 Single – Channel Ion channel reconstitution

A key method to study the structure-function relationship of a biological ion channel is to reconstitute isolated channel proteins into planar lipid bilayer membranes separating two aqueous compartments [22]. Theoretically it is possible for these 'artificial' membranes to mimic their natural counterparts and hence a study of the channel proteins under question can be undertaken in a controllable environment.

Principal strategies for such reconstitution experiments include the formation of lipid bilayer membranes using bulk solutions or monolayers [5] followed by a thinning process [23]. Both these methods can be employed for the incorporation of ion channels into the bilayers requiring a site across which the bilayers can be hosted. In this regard, several methods based on a two compartment setup have been proposed. The materials used as supports include glass [5], Teflon [20], and Silicon [9] [25] [32]. All these methods allow free access to the channel of interest and formation of Giga-seals [11].

1.2 Multi – Channel Ion channel reconstitution:

The single channel ion channel reconstitution has been proven to be a reliable method in which bilayers are formed and ion channel proteins are self-inserted to observe and study their properties [9] [12] [27] [32].

In the traditional method of 'painting', the thinning process of the bilayers that are formed is often unpredictable and the resulting bilayers may be fragile. In other cases the lipids may clump together forming a blob. In addition, the large scale of the system with bath volumes of several milliliters asks for a smaller sized system where the use of biological materials will not be excessive. This necessitates the use of smaller systems and a reliable method where lesser trials will be required to obtain a stable bilayer.

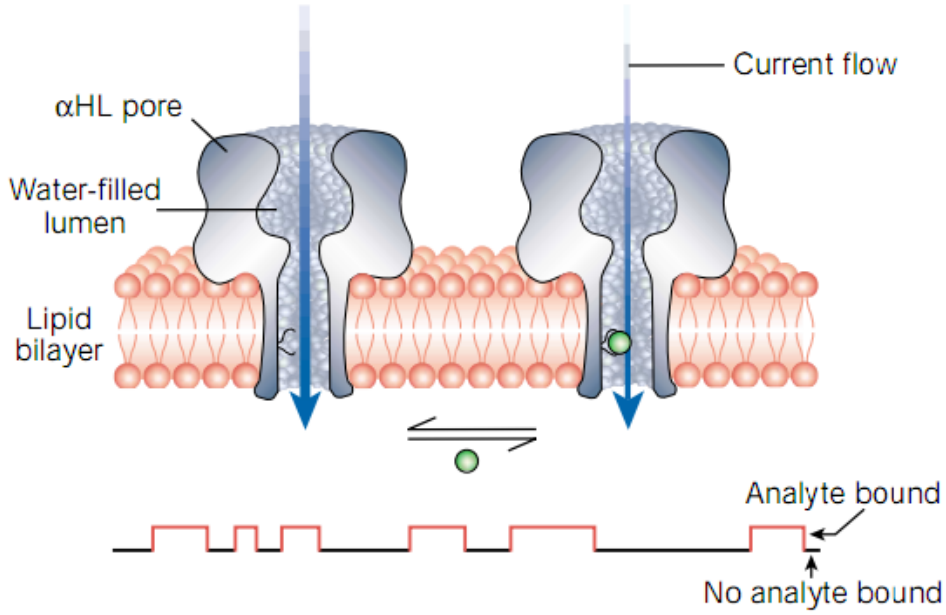

Figure 1. Stochastic Sensing with Engineered pores [4]

Applications of Nanopore Stochastic Sensing such as High Throughput Screening and ‘Electronic Nose’ require high sensitivity and discrimination with different affinities for analytes of interest [34]. This can be achieved by an array of specific single channel sensors. The events are detected as transient blockades in the current that is recorded. The frequency of the event reveals the concentration of the analyte. The duration and amplitude reveal the identity of the element.

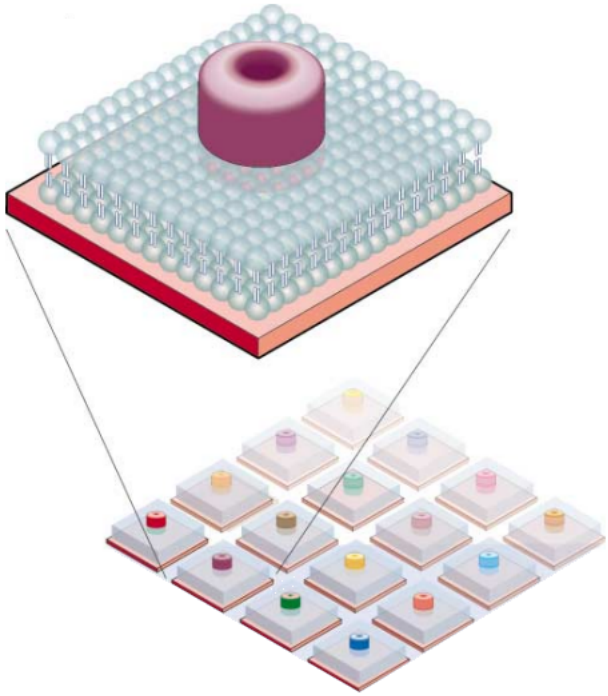

Figure 2. Conceptual Rendition of a Stochastic Array Sensor [4]

A number of platforms have been proposed for the arrangement of such an array and the recording of such signals in parallel. In most of these platforms an array of microholes is fabricated, which is used as the support for the lipid bilayer

membranes that are formed. Ion channels are self-inserted into the bilayer membranes and the ionic current signal from these parallel sensors are recorded and then processed by DSPs.

Even if more than one ion channel is active in each bilayer formed, it still enables recording of single channel events in a parallel fashion, assuming that the amplifier resolution is sufficient.

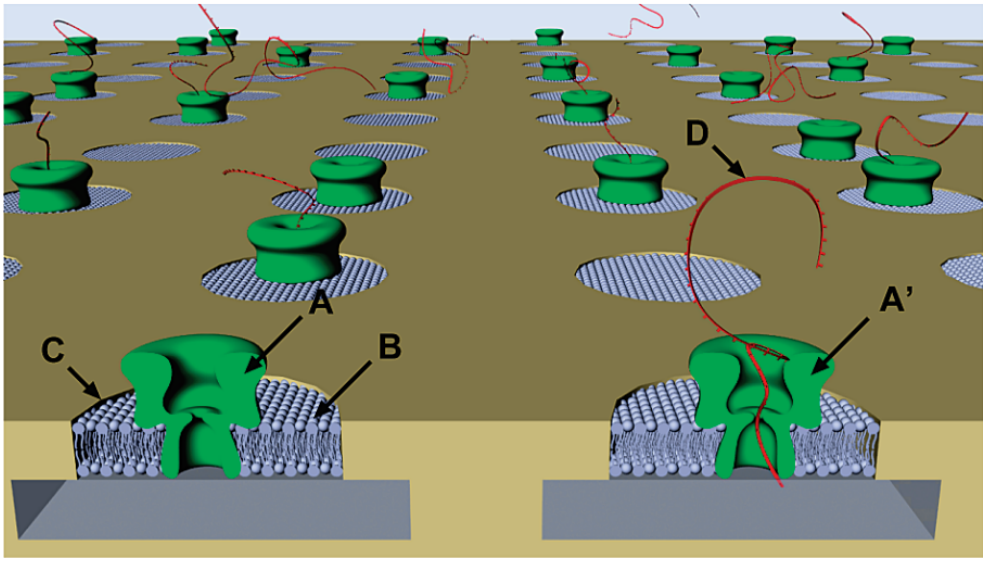

Figure 3. Parallel assay using α-Hemolysine nanopores [24]

A model of such a configuration is shown in Figure 3. In this case a parallel assay is made simultaneously in chambers C with lipid bilayers B, containing the ion channels A and A' in the absence and presence of a translocating molecule D respectively. In such a case it is important that each component sensor works independently of each other and is measured independently but also simultaneously.

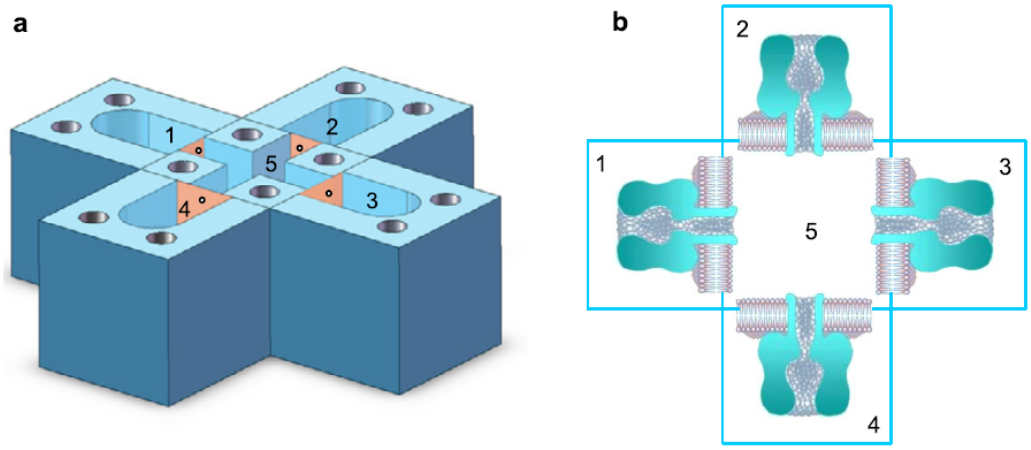

Figure 4. Illustration of a stochastic sensor with four sensing sites [34]

1.3 Anti-biotic translocation through OmpF membrane channels:

Several studies have described permeation processes in porins by antibiotics, such as ampicillin and amoxicillin. The outer membrane protein F, OmpF, is considered a major porin in the antibiotics pathway. [16]

The OmpF is a non-specific transport channel present in the outer membrane of E.Coli. While the outer membrane protects and separates the cell from the environment, OmpF is used for passive translocation of vital molecules and ions between the cell and the environment and allows the diffusion of molecules with molecular weights up to 600–700 Da. [16]

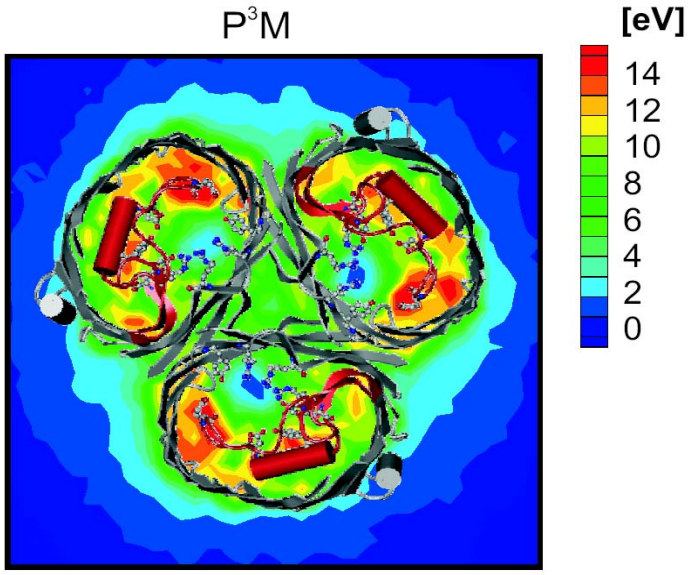

Figure 5. Potential Energy profile of OmpF [1]

The OmpF protein is constituted by three monomers forming a trimer. Each monomer consists of 16 β-strands anti-parallel that span the outer membrane and form a barrel with short turns at the periplasmic side and large loops at the outside of the cell. The porins have been shown to play a major role in the bacterial resistance against antibiotics.

Experiments have shown that the current analysis of the OmpF protein corresponds to a trimeric conductance, which have been verified from other studies [7] [16]. At high voltages, the porins exhibit monomeric gating. In addition, sub-conductance states have also been studied, which are much smaller than monomeric conductance states.

The effect of polyamines and antibiotics on OmpF activity have been studied and well documented. It has been shown that polyamines inhibit processes

such as chemotaxis by interaction with the L3 loop and barrel of OmpF [7] [33]. These studies are important as the presence of polyamines increases the ability of bacteria to maintain its potential when antibiotics are applied.

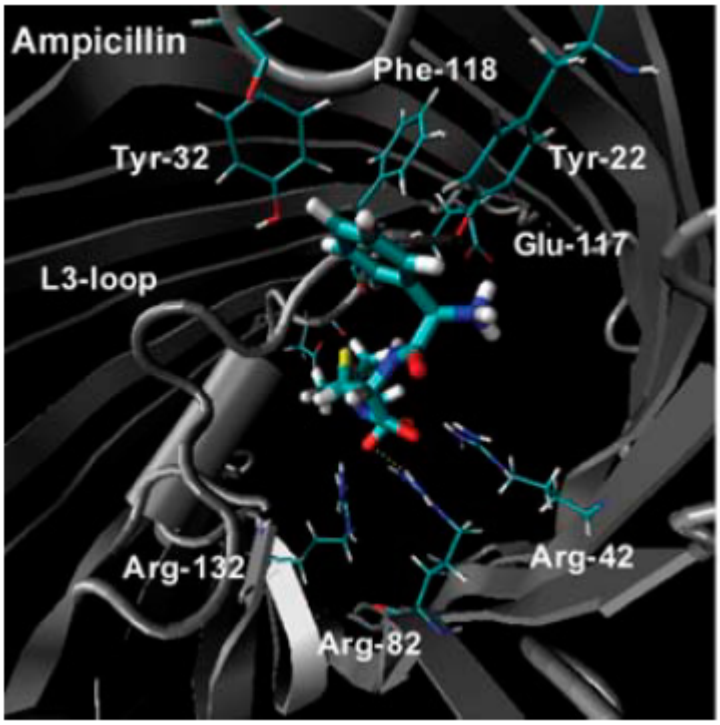

Figure 6. Simulated model of molecular dynamics of Ampicillin binding [7]

The presence of Ampicillin has been shown to cause current fluctuations in the ion current [7] [19]. This has been shown to be due to the translocation of the antibiotic through the protein. Additionally the residence time of the antibiotic inside the channel has been shown to strongly decay with temperature [19].

1.4 Multi-channel low-noise instrumentation amplifier and support circuit

The advancement of ion channel recording from multiple sites is heavily dependent on the availability of high throughput low noise multi channel amplifiers. The basic patch clamp amplifier is essentially a sensitive low-noise current to voltage convertor that can measure currents in the pA range that can be observed on an oscilloscope or sampled by a computer [27]. The headstage design usually consists of a pre amplifier stage with a dual JFET and an Op amp [11] [14]. JFETs offer a low voltage noise and input capacitance with low gate currents [10]. A number of commercial patch clamp amplifiers are available in the market; however, the number of available channels is limited.

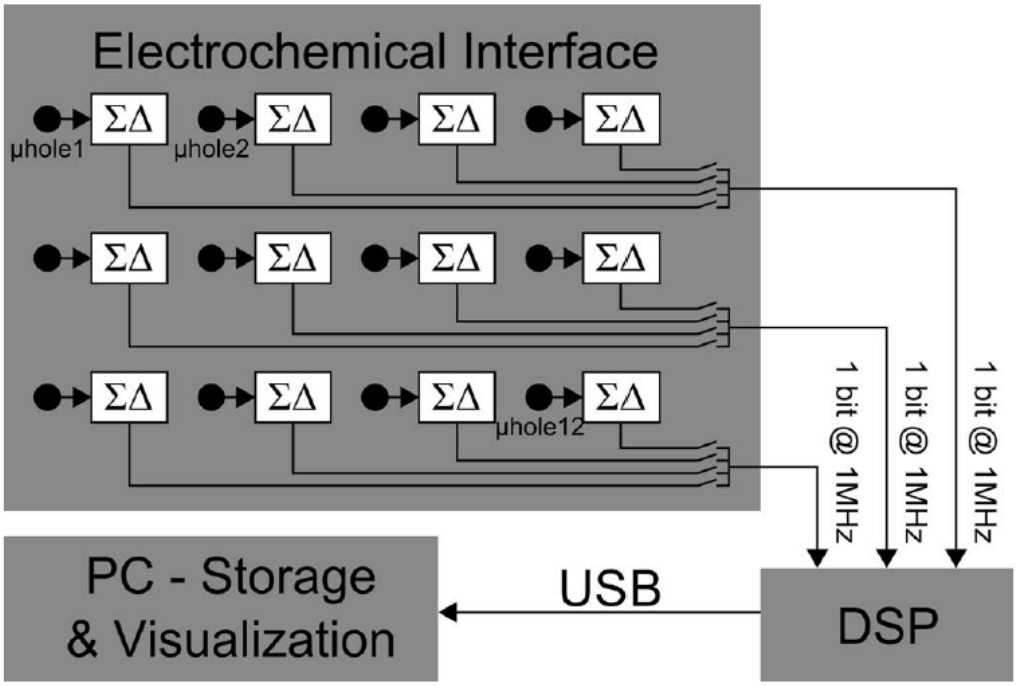

Figure 7. Structure of a system used for parallel recording of Ion channels [29]

It has been experimentally demonstrated that the presence of various parasitic capacitances such as electrode parasitic capacitance [13] [14] [17] [28] and parasitic capacitance across the feedback path [21] can affect the step response of the applied command voltage signal. Thus, the advantage of using a capacitance compensation circuit has been demonstrated by comparing uncompensated current recordings with compensated readings [15]. In addition the presence of junction potentials necessitates the need for pipette offset compensation.

In order to recover fast switching responses of the ion channel proteins, either the bandwidth of the resistive-feedback headstage has to be increased or a subsequent analog or digital correction circuit can be employed [21]. The former is a practically difficult solution to achieve, relying on wide-gain-bandwidth components which might have a negative impact on the Signal to noise ratio. For the latter, a frequency boost circuit is required to correct the frequency response of the headstage. This stage “replaces” the corner frequency due to the headstage with a new roll off at a much higher frequency.

Chapter 2

MATERIALS AND METHODS

2.1 Silicon Micropores:

Micropores can be created with the help of electrical spark discharges or mechanical drilling or fabricating in silicon. It offers the possibility to generate pores ranging from several hundred micrometers down to tens of nanometers. The process of forming bilayers is repeatable over a single substrate.

Silicon is a very well characterized material in the semiconductor industry, with the benefit of being biocompatible. It also allows the monolithic integration of electronic components on the same sensor chip. The process steps needed for silicon micro fabrication are well-established and thus readily available and cost effective. However, Silicon faces some issues which hinder the process of forming bilayers effectively. Silicon dioxide is hydrophilic, thus preventing high resistance bilayer seal formation. To remedy this situation, the silicon dioxide surface is made hydrophobic by chemical vapor deposition of a polytetrafluoroethylene (PTFE) layer. Another issue is that the capacitance of oxidized silicon is higher than that of other substrates, e.g. glass or plastics. This matter can be resolved by adding passivation layers made of SU-8 which lowers the substrate capacitance.

Double-sided polished Si (100) wafers with a thickness of 380-420 μm were used for our experiments. A recess etch was performed to thin down the area

around the central aperture. This enables thinning of lipid bilayer. The area for the back-side etch was photolithographically defined. A deep reactive ion etch (Bosch process) to prepare the recess. Using back side alignment, bilayer apertures in the range 5 μm and 50 μm were defined photolithographically and etched using the deep reactive ion etch process again. The back side of the wafer was coated with SU-8 of a thickness of 40 μm respectively, with a central area of 100 μm removed around the final aperture. Then, the surface was coated with a plasma-polymerized PTFE layer using the ICP tool. Thereafter, the wafer is diced into individual pieces each holding a single aperture.

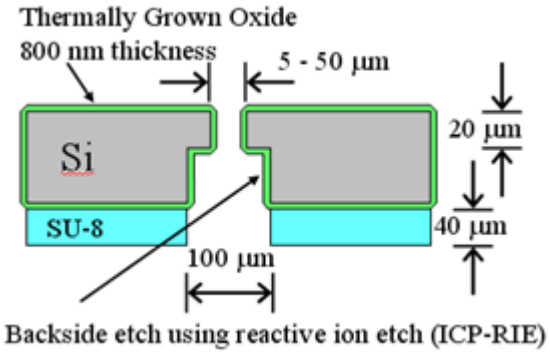

Figure 8. Illustration of the cross-section of a silicon micropore

The reactive ion etch used in this design is very precise and allows for close spacing of pores. As shown in figure, SU-8 does not need to cover the edge of the back side pore. A thick PTFE layer enables high seal resistance and smoothens out micro-roughness. A disadvantage of reactive ion etching is a

conflict between etching rate and anisotropic profile. An increase in etching rate leads to increase in concentration of reactive species thereby generating higher gas pressure and more collisions – implying a weaker anisotropic profile. Therefore, dry backside etch shows depth and feature size dependent etch rate decrease.

For our experiments 4 silicon micropores with aperture diameters of 30 um were used.

2.2 Preparation of Electrolyte solution

Potassium chloride (KCl) buffer at concentrations of 1 M and 0.5 M was used for the bilayer measurements without and with Ampicillin respectively. These were buffered with 10mM N-(2-hydroxyethyl) piperazine-N'-(2 ethanesulfonic acid) (HEPES). The molecular weight of KCl is 74.55 g/mol while that of HEPES is 238.31 g/mol. Thus, the amounts of KCl and HEPES required for preparation of 1.0 M KCL solution were 18.638 g and 4.766 g respectively. Since the HEPES added makes the solution acidic, the pH of the solutions needs to be increased. The final solution was titrated to a pH of 7.4 using 1.0M potassium hydroxide (KOH) solution.

2.3 Device Mounting:

A device was designed for mounting the Silicon micropores in a vertical array. The holder was designed using Solidworks and machined using acrylic and has two main compartments.

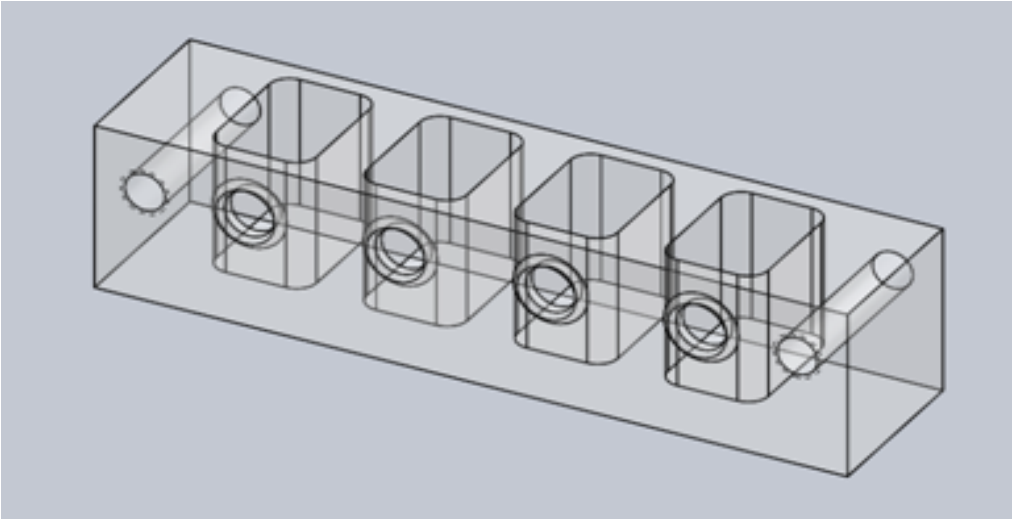

Figure 9. Design of the 4 well silicon chip holder

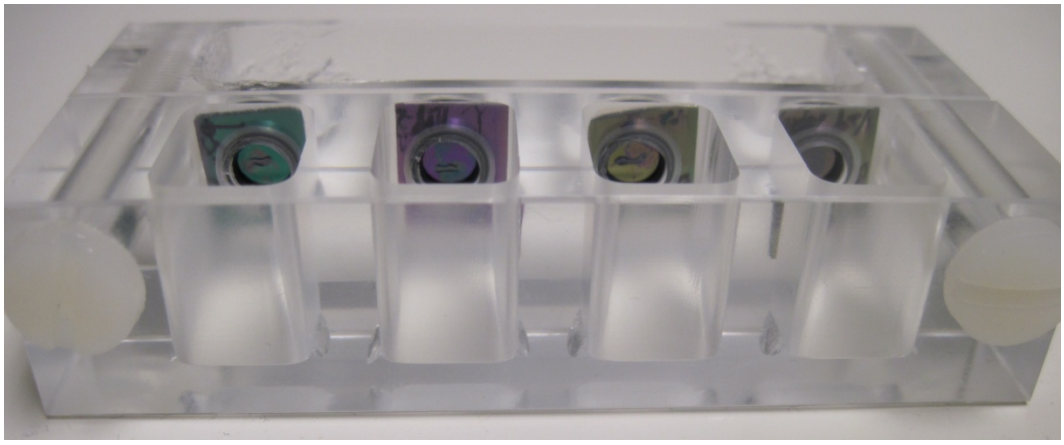

Figure 10. Acrylic based 4 well holder mounted with 4 silicon micropores

The front compartment where the micropores are painted with lipids are divided into four sub compartments, thus making an array of four compartments for

mounting four silicon micropores vertically. The back compartment is common to all four micropores.

Both compartments have four equally spaced 5 mm countersunk holes to fit Viton ® fluoropolymer elastomer gaskets. The countersunk holes serve as windows to paint the micropores easily. The silicon micropores are sandwiched between the gaskets to obtain a watertight assembly. The whole assembly is then tightened with acrylic screws.

2.4 Low Noise Amplifier:

The amplifier used is basically a current- voltage converter. The most important property of such an I-V converter is to maintain a high gain (approximately 80 dB) while maintaining low noise amplification from DC to around 100 kHz. The designed amplifier has four channels that measure the current through the ion-channels parallel at the same time. The amplifier is designed to do a voltage clamp measurement, in which case the transmembrane potential is kept constant and the current through the ion-channel is measured.

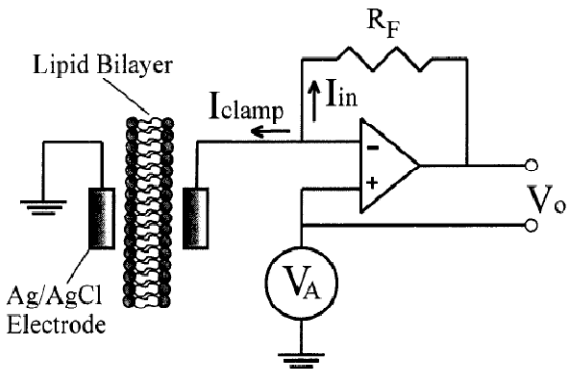

Figure 11. A simple arrangement depicting a patch clamp arrangement

The positive and negative inputs of the op amp are forced to the same potential so the applied potential (V_A) is held constant across the membrane. The current flowing out of the op-amp (Iclamp) is equal to the current flowing into it (Iin). All the current flowing through the feedback resistor Rf can be determined such that:

$$V_{out} = I_{clamp} R_f \tag{1}$$

Where Vout is the measured output voltage and Rf is the feedback resistor determining the gain of the circuit. The current flowing through the membrane can then be easily using the known value of the feedback resistor and the measured voltage output. The strategy employed is to use a high gain-bandwidth amplifier and to limit the stray capacitance to an acceptable value. Nevertheless, due to the high gain requirement in the first stage to limit the noise, the bandwidth will be limited. With the amplifier having a well-defined frequency characteristic,

it is possible to correct for a gain roll-off at a later stage, using a frequency boost circuit. In all designs and revisions of the PCB that were fabricated, the Sigworth design was adapted. [27]

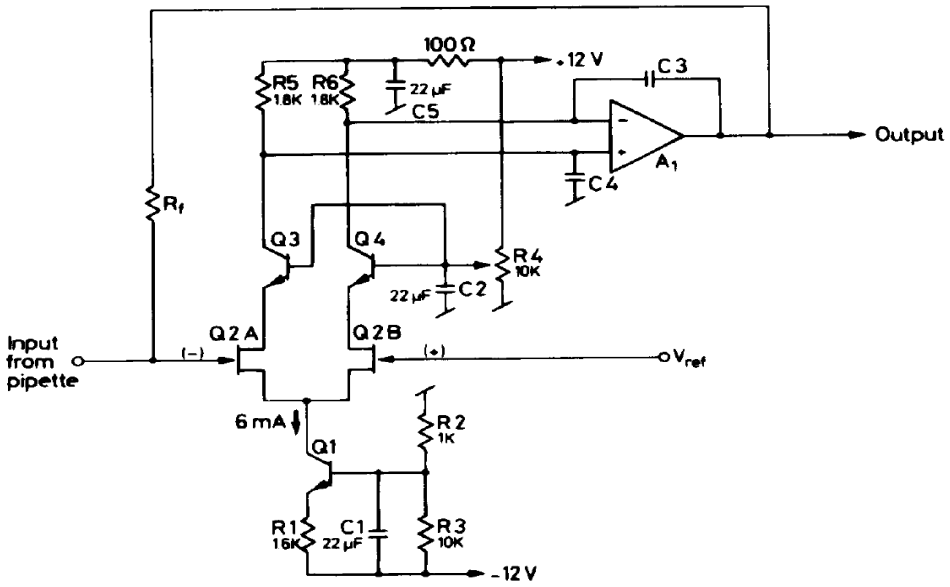

Figure 12. Schematic diagram of a current to voltage converter [27]

All components used in the designed board are currently in production. All JFETs, BJTs and Op amps used in the board are surface mount components, minimizing the parasitic influence of inductance, capacitance and dielectric noise at feedthroughs. In this design a dual JFET Q2 is used in a differential preamplifier, the output of which is amplified by the Op amp A1. Transistor Q1 acts as current source for the JFET amplifier. The transistors Q3 and Q4 set the drain voltages and isolate the load resistors R5 and R6 from the drains.

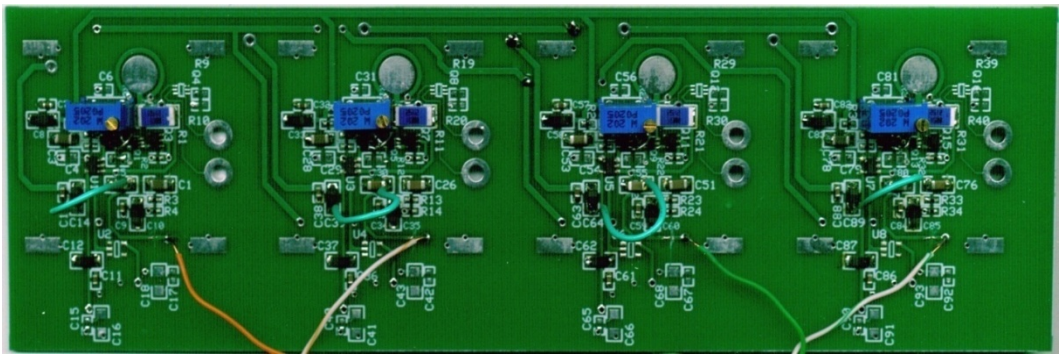

Figure 13. Four channel headstage amplifier (version 1)

The design was implemented using a two layer PCB. All four amplifiers were on the same board in the first design, with connectors for five Silver/Silver Chloride electrodes.

2.5 Electrode Properties

A common method for measuring transmembrane currents is to use reversible silver/ silver chloride (Ag/AgCl) electrodes which follow the reaction:

$$AgCl(s) + e^{-} \rightleftarrows Ag(s) + Cl^{-}(aq) \qquad (2)$$

This reaction is a redox reaction because at the cathode the AgCl electrode is reduced and the anode the electrode is oxidized. The standard reduction potential of the half cell reaction in equation (7) is +0.2223 V. Thus, the standard reaction potential of the system would be:

$$E^{0}_{cell} = E^{0}_{reduced} - E^{0}_{oxidized} = 0.2223V - 0.2223V = 0V \qquad (3)$$

Thus, the concentrations of both baths are the same, in this case 1M, the Nernst potential of the system is 0V:

$$E_{cell} = E^{0}_{cell} - \frac{0.0592V}{n}\log Q = 0 - \frac{0.0592V}{n}\log\frac{1}{1} = 0V \quad (4)$$

where Q is the reaction quotient.

In our experiments, silver wires were commonly used to make the Ag/AgCl electrodes. The Teflon insulation from the ends of silver wires was stripped and then the silver ends were inserted into common household bleach (5% NaOCl) until a thick layer of AgCl formed on the wires (usually for ~15 minutes).

AgCl forms a white colored salt that is oxidized in light and changes to a black color. It is important that the ends of the wires are completely chloridized or covered with the Teflon insulation so that no bare silver is in contact with solution otherwise electrode potential would drift [27].

2.6 Syringe Pump for Automatic Bilayer Formation:

In order to show that bilayers can be automatically formed in all four apertures at the same time, a proof of concept was performed using a programmable syringe pump (Harvard PHD 2000). The method used in this case is the Montal – Mueller method, where the solution of lipids with the buffer solution is raised and lowered repeatedly in the chamber. The lipids at the air – water interface then form a bilayer across the aperture.

Figure 14. Harvard PHD 2000 programmable syringe pump

The pump employs a microcontroller that controls a small step angle stepping motor that drives a lead screw and a Pusher Block. Data can be entered using the keypad or via the RS 232 connector located on the rear panel. The microcontroller, using the internal Syringe Look-Up Table, calculates the cross-sectional area of the syringe selected and calibrates the flow rate and volume accumulation [26].

The pump operates in three modes of operation: Pump, Volume and Program modes. In pump mode the motor runs continuously in infuse or refill directions until stopped. In the volume mode the pump runs until a particular volume has been pumped or refilled. In the program mode the pump follows a specified sequence of instructions.

2.7 Measurement Setup and Noise considerations

Since the current signal to be measured is on the order of picoamperes, the signal-to-noise ratio has to be sufficiently large so that signal does not get buried under noise. Experimental measurements are conducted in the same frequency range as equipment power supplies and general lighting in the room. The measurements are also affected by mechanical vibrations of the system. To carry out low noise measurements, it is of utmost importance to build a measurement setup that is electrically isolated, properly grounded and mechanically stable.

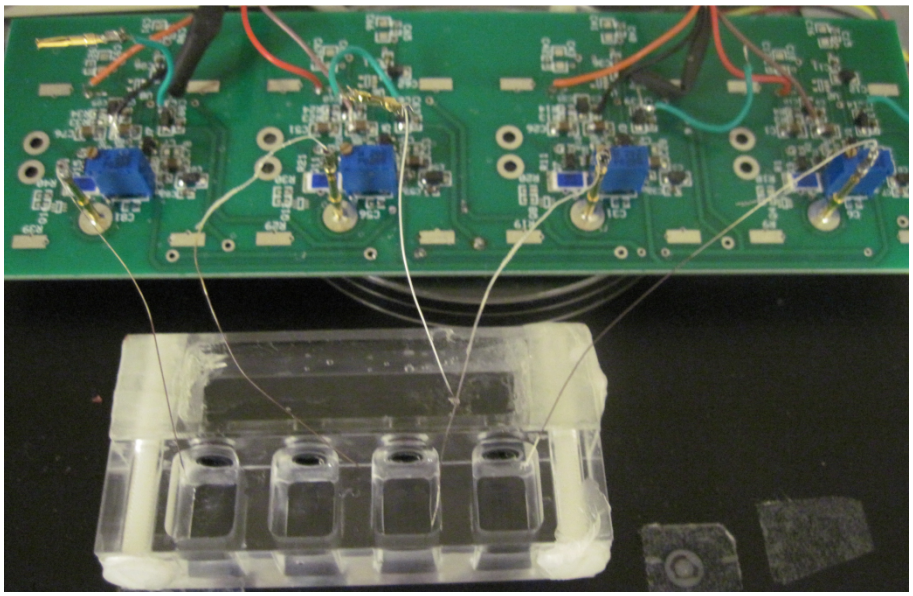

Figure 15. Acrylic holder with headstage amplifier, inside the Faraday cage.

These low voltage measurements are sensitive to 60 Hz noise. With no shielding, one would see periodic 60 Hz noise spikes in the output current signal; thereby distorting it. Hence, a Faraday cage was used in shielding the bilayer

system from electromagnetic radiation. A metal locker which was properly grounded served as an effective Faraday cage. The noise sources include overhead lighting system in the room, computer monitors, amplifier power supplies, transformers, switch mode power supplies and any switching elements in the vicinity of the bilayer system.

Mechanical vibrations are also detrimental to measurements. Major sources of mechanical vibration include people walking near the setup, audible conversations, people working on the same lab bench on a different area, cooling systems, small stir bar used in bilayer experiments and opening and closing of Faraday cage. An active isolation vibration table from Halcyonics was employed in removing effects of mechanical vibrations. In an active vibration control set-up, the signals acquired by extremely sensitive vibration detectors are analyzed by electronic circuitry driving electro-dynamic actuators which instantaneously produce a counter-force to compensate for the vibration. The active damping system has no resonance and no amplification of vibrations at any frequency.

A single ground point is also important to prevent noise due to ground loops between different parts of the setup [13]. All metal equipment including the patch clamp amplifier headstage, the Faraday cage and the anti-vibration table should be electrically connected to a single point to prevent ground loops due to different paths to ground. A ground loop would enable a magnetic field to induce

a potential difference between different points, for example, the bilayer ground and the electronics ground, resulting in a large excess noise current [28].

2.8 Forming the bilayers:

Lipid bilayers are formed across the apertures using two methods. In the bubble collapse method, each aperture was individually painted by bubble collapse at the tip of a pipette containing the lipid solution. Care is taken in painting an aperture that the bilayers already formed in the other apertures are not destroyed. Forming parallel bilayers by this method requires a lot of time as each pore has to be individually painted. In addition, there is a chance of damaging the PTFE layer on the front face due to scratching by the pipette tip.

The second method based on the Montal-Mueller method provides an automatic way of forming bilayers using a syringe pump.

Chapter 3

EXPERIMENTAL SETUP

3.1 Designing the array mounting device

The biggest hurdle in the past for performing ion channel reconstitution experiments using multiple silicon chips in parallel was the lack of availability of leak-proof holders to sandwich the silicon microchips between the cis and trans chambers without having to use silicone glue. In order to overcome this, a four channel holder was designed using Solidworks as described in Chapter 3. As the holder has been fabricated from an 18mm x18 mm solid acrylic rod there is no possibility of leakage between the individual channels. The Viton ® fluoropolymer elastomer gaskets ensure leak-proof seal between the cis and trans sides of the holder. This eliminates the possibility of "cross-talk" between individual channels due to solution leakage.

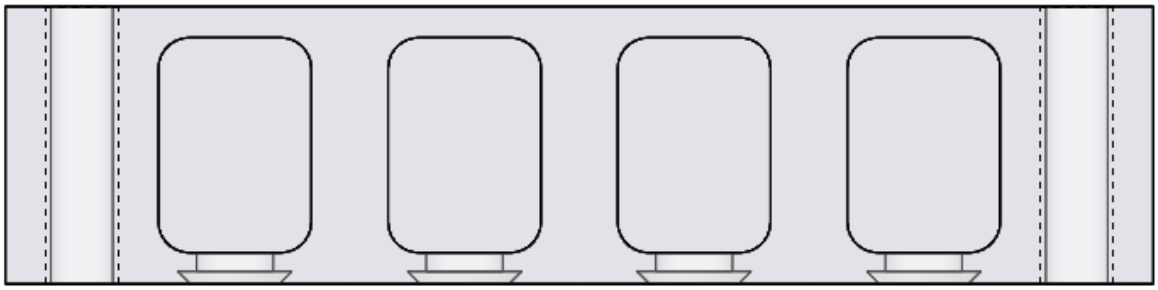

Figure 16. Top view of design of multi-well chip holder in Solidworks

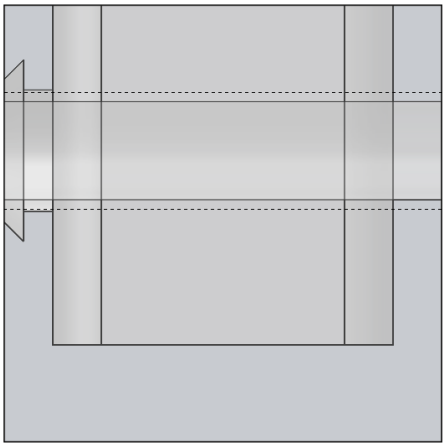

Figure 17. Side view of acrylic holder showing the groove for the gasket

Another aspect that was taken into consideration was the mounting of the chips. Mounting can be done horizontally [6] or vertically. In this design a vertical configuration was adopted because of the ease of forming lipid bilayers using either the bubble painting or the Montal-Mueller method. A horizontal configuration would require the design of a microfluidic system or the use of vesicle fusion.

3.2 Headstage amplifier design

The new headstage PCB design is based upon an earlier design that has been improved upon to allow a more compact and modular setup. One important design requirement was the bandwidth of the headstage. The bandwidth should be wide enough to observe the gating signals of ion channels that are being studied. To be able to digitize the ion channel gating signals, the headstage amplifier has to be set to a gain of 90dB.

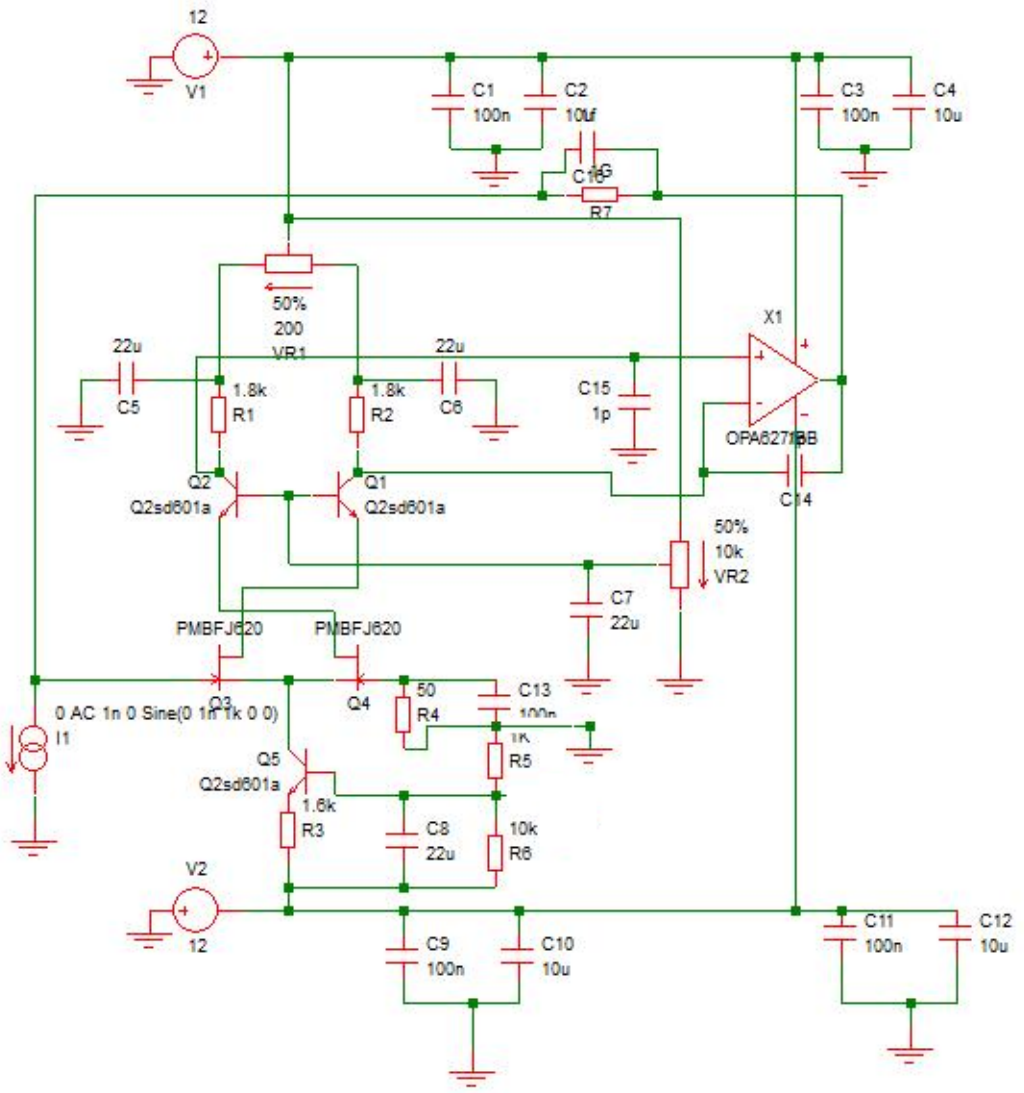

Figure 18. Schematic diagram of simulated headstage amplifier

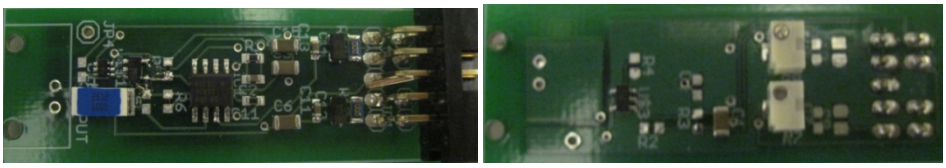

Figure 19. Front and back view of Headstage amplifier (version 2)

Based on the previous design, a smaller, more compact PCB was made and was tested. The frequency response was obtained using a Keithley 6220 AC Current source programmed using Labview, to generate a frequency sweep over the frequency range of 1 Hz up to 20 kHz. The Op amp used in the headstage amplifier has to be selected keeping in mind the Gain – Bandwidth product and noise considerations. For this purpose four Op-amps were chosen based on Gain – Bandwidth product, noise specifications, cost considerations and operating voltage. A selection of Op-amps used for testing the boards is listed in Table 1.

The OPA 134 is an inexpensive FET input, audio Op amp also available in a quad configuration. The OPA 656 is a FET input ±5V Op amp with a high Gain-Bandwidth product. The OPA 827 is a JFET – input Operational amplifier and the TLE 2037 is a low noise high speed bipolar Op-amp. As a comparison, the values for the two amplifiers suggested in the design by Sigworth [27] are listed (NE 5534 with bipolar input and LF 356 with JFET input).

Table 1

Typical values of Gain-Bandwidth and noise specifications of Op amps used in the Headstage Amplifier

Op – Amp (Technology)	Specified Operating Voltage (V)	Gain – Bandwidth Product (MHz)	Input Voltage Noise Density nV/√Hz	Input Current Noise Density fA/√Hz
OPA 134 JFET	±15	8	8 (at 1 kHz)	3 (at 1 kHz)
OPA 656 JFET	±5	230 (for Gain>10)	7 (>100 kHz)	1.3 (>100 kHz)
OPA 827 JFET	±4 to ±18	22	4 (at 1 kHz)	2.2 (at 1 kHz)
TLE 2037 Bipolar	± 15	50	2.5 (at 1 kHz)	400 (at 1 kHz)
NE 5534 Bipolar	± 15	10	3.5 (at 1 kHz)	400 (at 1 kHz)
LF 356 JFET	± 15	5	12 (at 1 kHz)	10 (at 1 kHz)

3.3 Support Circuit Design

Commercial patch-clamp amplifiers such as HEKA and Axopatch employ a "support circuit" after the headstage, which subtracts the command voltage from the output signal, provides offset and gain correction as well as a compensation for the frequency response of the headstage. In our case, it is desirable to have "support circuits" for each of the headstage amplifiers. Hence, such a control circuit was designed and simulated with the critical parameter being the gain equalization circuit.

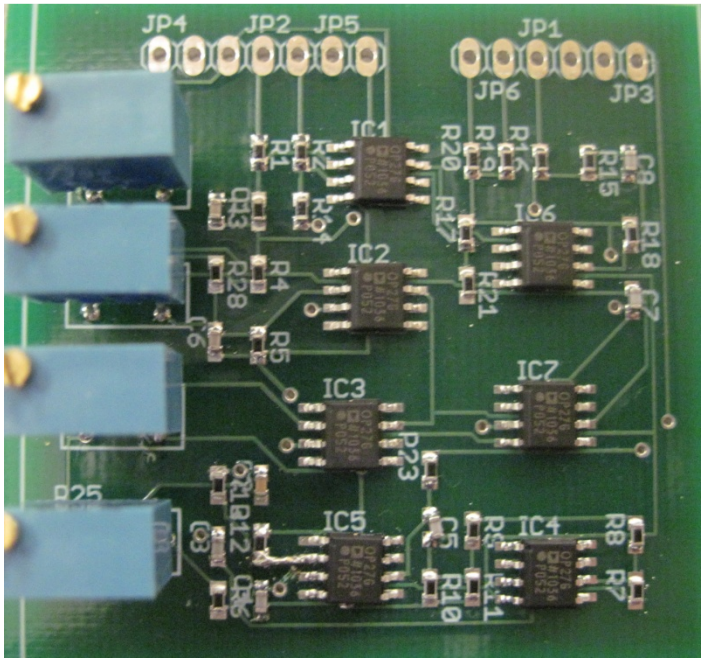

Figure 20. Support circuit used with the headstage amplifier

The support circuit is modeled after similar circuits found in commercial amplifiers and what has been published in [28] (Sigworth 1994, 1995. EPC9).

The support circuit provides two main functions: 1) Gain and Offset correction and 2) Frequency Boost. In addition to these functions, the circuit terminates with a Bessel filter so that the response rolls off at 10 kHz. This value was chosen to be around 10 kHz with the sampling rate being 100 kHz in accordance with the Nyquist criterion. A preceding stage includes a summing amplifier for Command voltage, Pipette Offset and Zap signals.

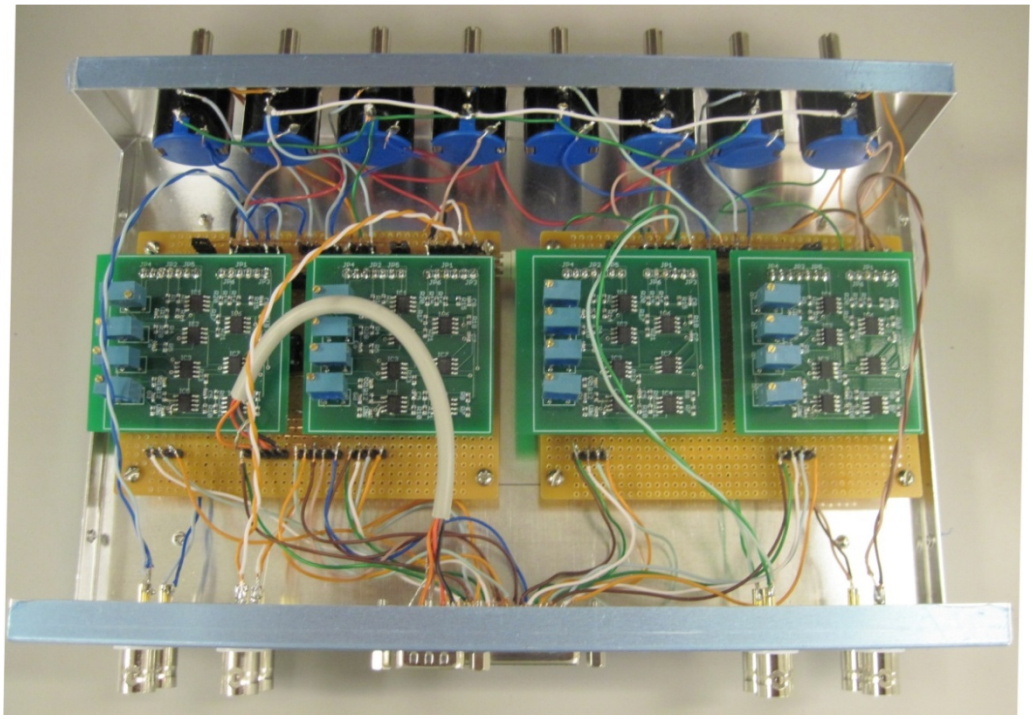

Figure 21. Support circuits with capacitance compensation

3.4 Automatic Bilayer formation using Harvard Syringe Pump

To accomplish automatic bilayer formation, a Harvard syringe pump is used, which is controlled via a LabView program. The pump is operated in the volume mode with the Target volume set as the volume of the chamber to be filled or to be emptied. While the front chamber is being filled with solution, a triangular voltage stimulus is applied and the amplifier monitors the current across the aperture, which is being acquired by the computer using a National Instruments board and processed to give a capacitance reading. This acts as feedback to operate the pump. If the bilayer has formed, the appropriate capacitance and resistance values are reached and the pump operation stops. If an electrical short between the chambers is detected, the pump reverses its motion, lowering the liquid level over the micropore until the level drops below the aperture and the electrical connection is removed. This concludes an iteration cycle at which end the direction of motion of the motion block reverses again. This cycle of repeatedly filling and emptying the chamber in which the bilayer is to be formed continues until a bilayer formation is detected. The infuse rate and refill rate are set to be synchronized with the time taken by the Labview program to perform a single iteration of capacitance and resistance measurements.

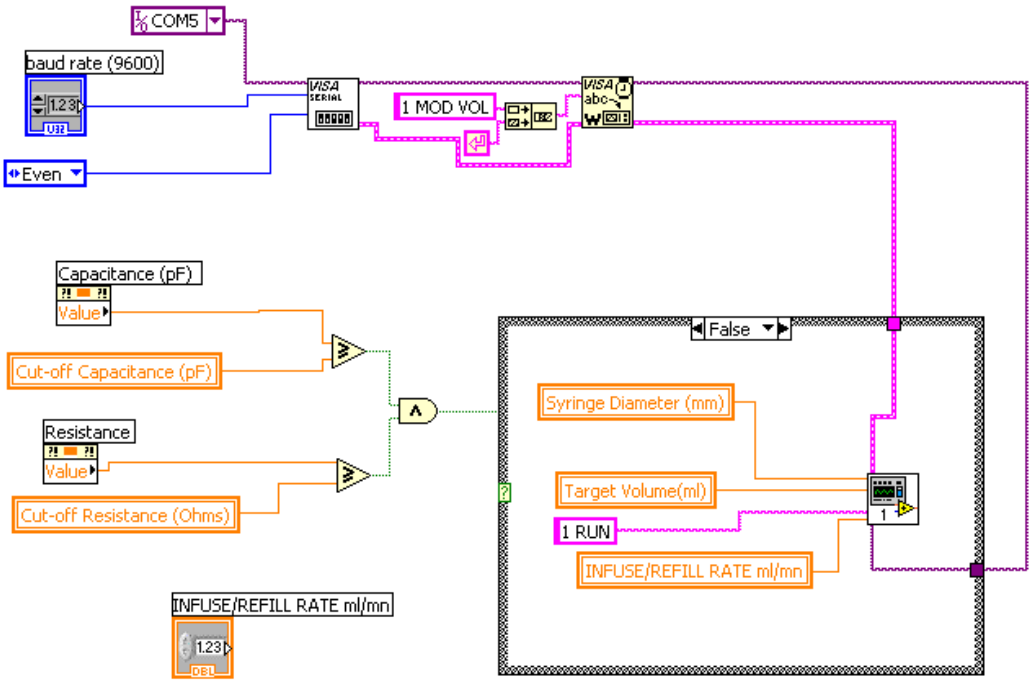

Figure 22. LABVIEW block diagram of Harvard syringe pump control

3.5 Frequency Response Measurement Setup

The frequency response of the headstage is necessary to study the variation of gain across the operating frequency range with the four Op-amps (Table 1) under consideration and to compare their performance. This requires an AC current to be swept across the chosen frequency range at the input of the headstage. In the case of this transimpedance amplifier the input is a current while the output measured is a voltage.

The Gain of an amplifier is expressed as,

$$Gain = \frac{Output\ Voltage\ (V)}{Input\ Voltage\ (V)}$$

In the case of the headstage transimpedance amplifier,

$$Gain = \frac{Output\ Voltage\ (V)}{Input\ \ Current\ (A) x\ Impedance\ (Ohms)}$$

However, the input impedance of the headstage is a sum of resistive and capacitive components. The capacitive component is frequency dependent which makes the Gain a frequency dependent quantity. Hence, the Gain of the transimpedance headstage circuit is given by

$$Gain(\omega) = \frac{Output\ Voltage\ (V)}{Input\ \ Current\ (A) x\ Impedance\ (\omega)\ (Ohms)}$$

This means that the input current is normalized by an impedance factor to express the gain of the circuit in dB.

In our case, we can express the Gain at DC or at a low frequency of 100 Hz as a dimensionless quantity by using a normalization factor of 1 mV/pA (1 GΩ).

$$Gain\ = \frac{OutputVoltage(Volts)}{Input\ Current\ (pA) x\ 1\ mV/pA}$$

To supply 1 nA of current at the input of the headstage, a Keithley 6220 AC/DC current source was used. Since the instrument does not have a built-in frequency sweep capability, it was programmed using LABVIEW to generate a

frequency sweep over a frequency range from 100 Hz to 10 kHz as shown in Figure 23.

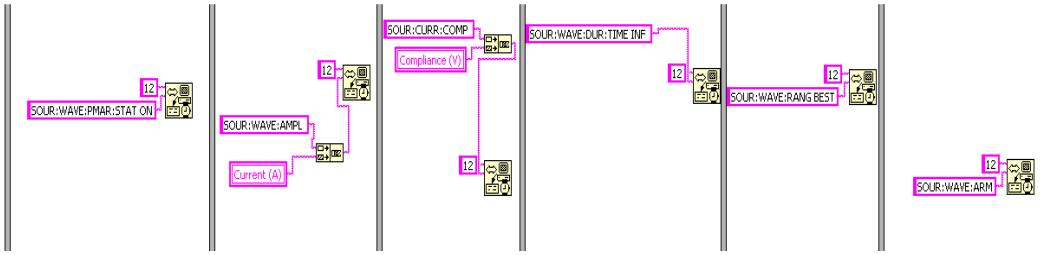

Figure 23. Initial setup for Keithley 6220 AC/DC current source in LABVIEW

The AC current source does not take into account the capacitive effects of the input impedance; it rather supplys a current of 1 nA irrespective of the phase relation between current and voltage. Since at high frequencies the capacitive component dominates, the source voltage will be lowered to maintain 1 nA of source current. In a practical application of voltage clamp, this is not the case, since the input only sees a constant voltage. To account for the difference in supply voltage for different frequencies, both the input and the output voltage are recorded simultaneously, using two synchronized lock-in amplifiers. The block diagram of the setup used is shown in Figure 24.

The SRS 830 Lock-in amplifier uses the trigger link from the Keithley 6220 AC current source as a reference input. The guard signal from the current source is fed to the input channel. Similarly, the trigger link from the current source is also used as a reference by the second lock-in amplifier (EG & G 5206), with the output voltage from the headstage at the input channel. The RMS

voltages from both lock-in amplifiers are then recorded and displayed in the Labview program.

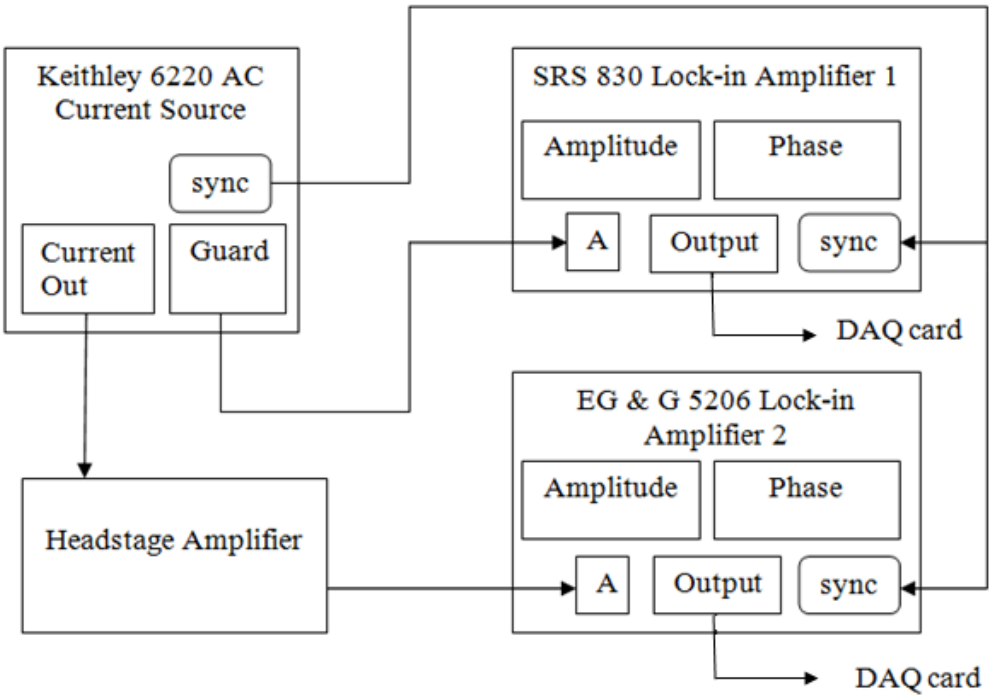

Figure 24. Block diagram of frequency response measurement setup

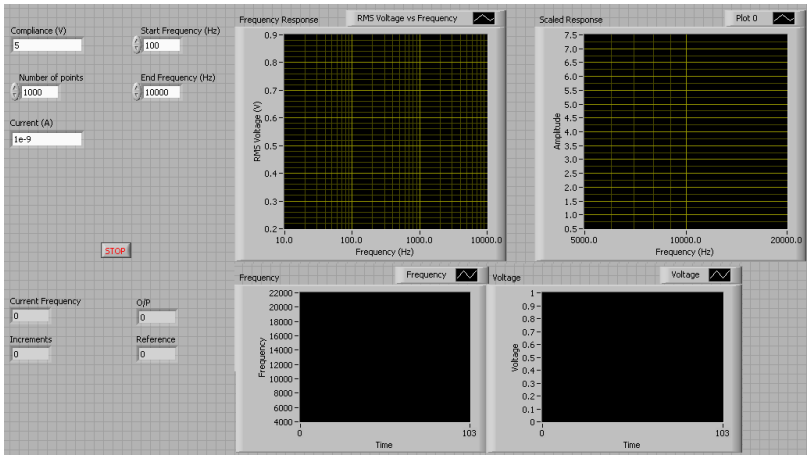

Figure 25. Front panel of the Labview VI for frequency response setup

The Labview program sweeps the frequency setting of the Keithley 6220 AC current source from 100 Hz to 10 kHz according to the number of points entered in the front panel. When the program reaches the end frequency of 10 kHz at the end of the first iteration, the program initiates a small delay and then starts the next iteration from start frequency. The delay is provided to ensure that the Lock-in amplifiers lock-in to the signals being measured in spite of the sudden jump in frequency from 10 kHz to 100 Hz. (Figure 26)

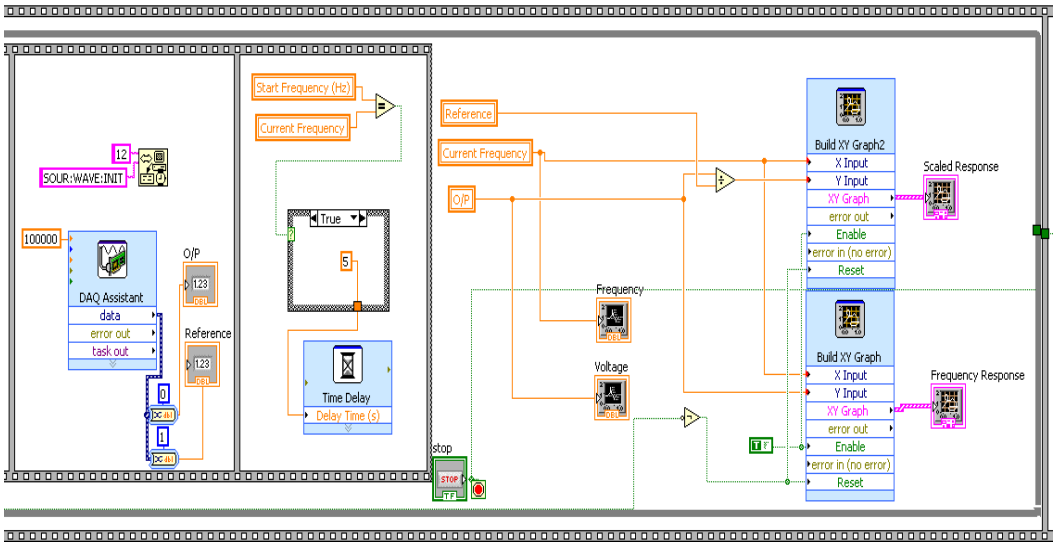

Figure 26. LABVIEW diagram for measuring the Frequency Response

Chapter 4

RESULTS

4.1 Array mounting device

The array mounting device was designed keeping in mind the necessity to separate the four channels and avoid cross-talk between the channels. This was successfully demonstrated by using a machined device out of a single acrylic rod. However, the mounting device faces cracking due to stress at the screw joints.

In order to prevent these problems the design was modified in Solidworks to make a physically isolated array in both the *cis* and *trans* sides of the holder. The design was also modified to accommodate two additional chambers making it a 6 chamber array as shown in Figure 27.

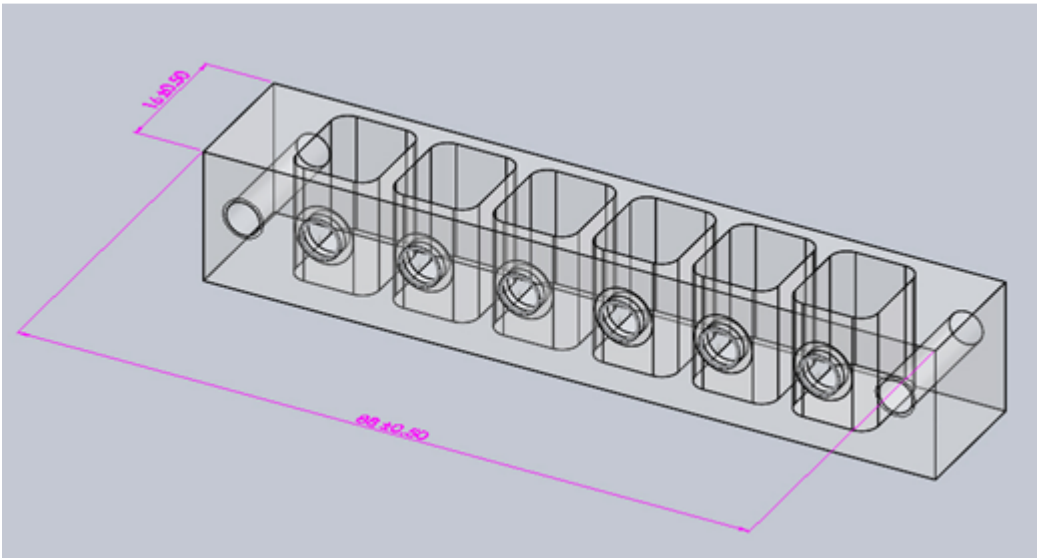

Figure 27. 3D model of cis side of the proposed 6 chamber silicon chip holder

4.2 Headstage Amplifier board

4.2.1 Design

The variable resistor VR2 offers a convenient way set the drain voltage of the JFET for the best noise performance. The simulation was performed by varying VR2, with the four Op-amps listed in Table 1 and the results are shown in Figures 28 – 31.

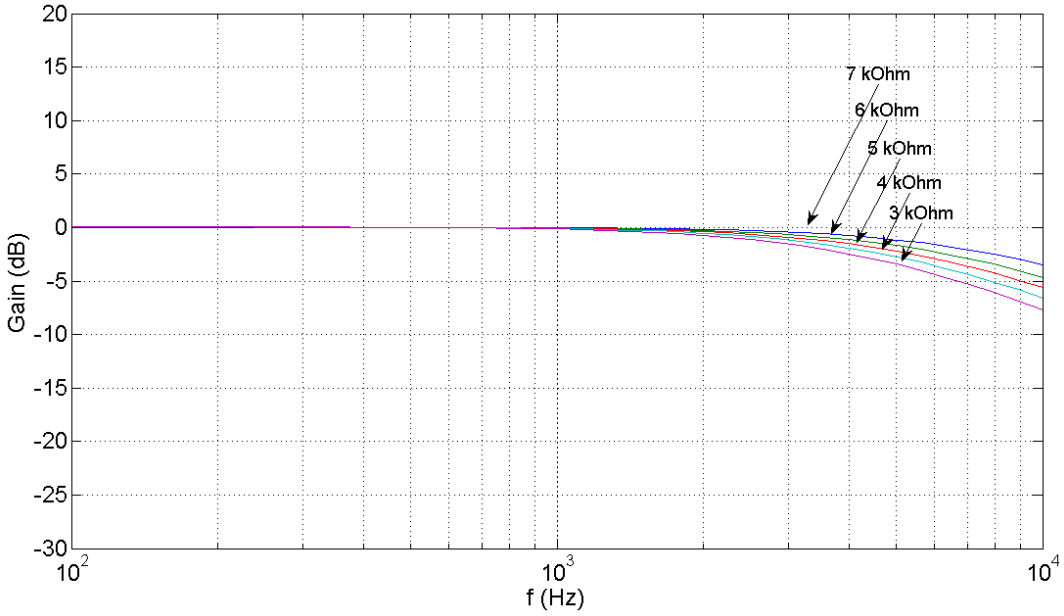

Figure 28. Simulated Frequency Response of Headstage amplifier with OPA 656

In the case of the headstage amplifier with OPA 656 the variation in the frequency response is not huge, and no frequency "ringing" or oscillation is observed at higher frequencies. However the response starts to roll-off at frequencies in the order of 10 kHz with slight increases in bandwidth with increasing VR2.

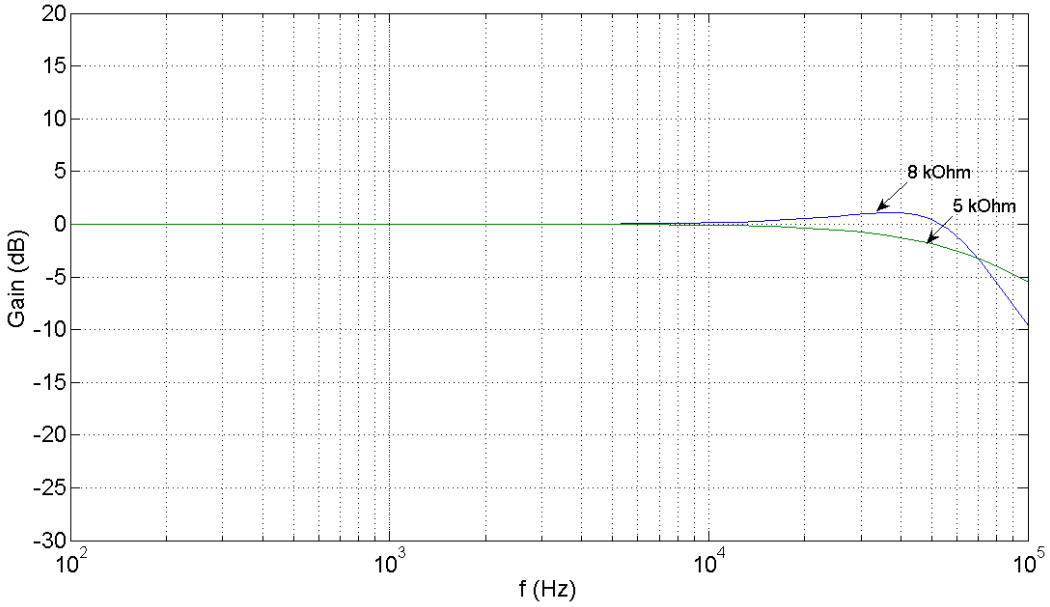

Figure 29. Simulated Frequency Response of Headstage Amplifier with OPA 827

In the case of the headstage amplifier with OPA 827 a wider bandwidth upto 10 kHz could be achieved. However when VR2 is set at 8 kOhms or above, a frequency hump is observed, indicating oscillations in the circuit. Similarly in the case of the circuit employing OPA 134, a larger bandwidth in the order of 50 kHz could be achieved; however the circuit oscillates at VR2 set below 5kOhm. The TLE 2037 shows a bandwidth of around 50 kHz with oscillations setting in below a VR2 setting of 4 kOhm.

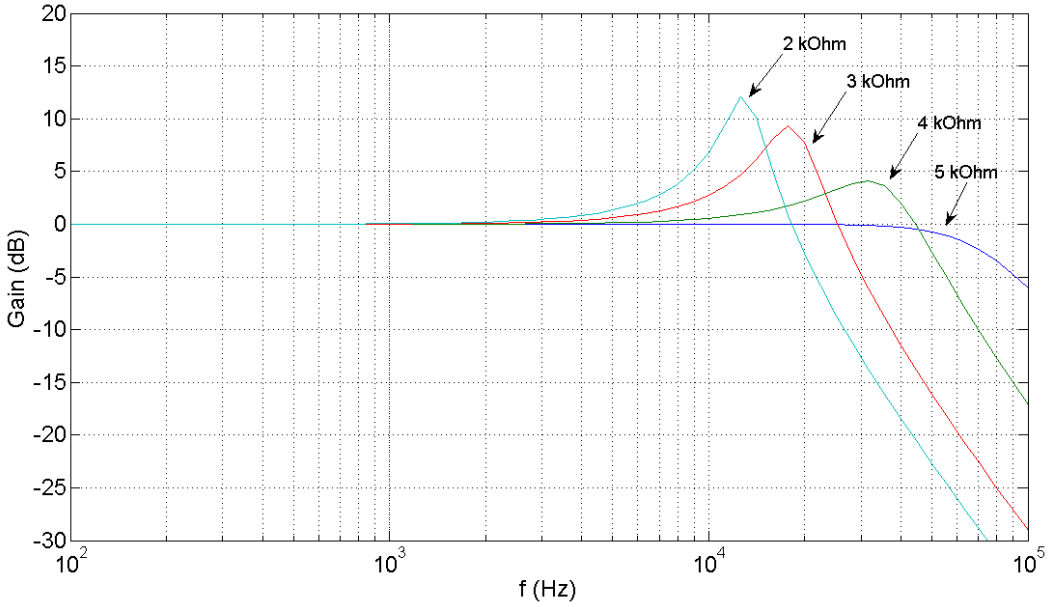

Figure 30. Simulated Frequency Response of Headstage Amplifier with OPA 134

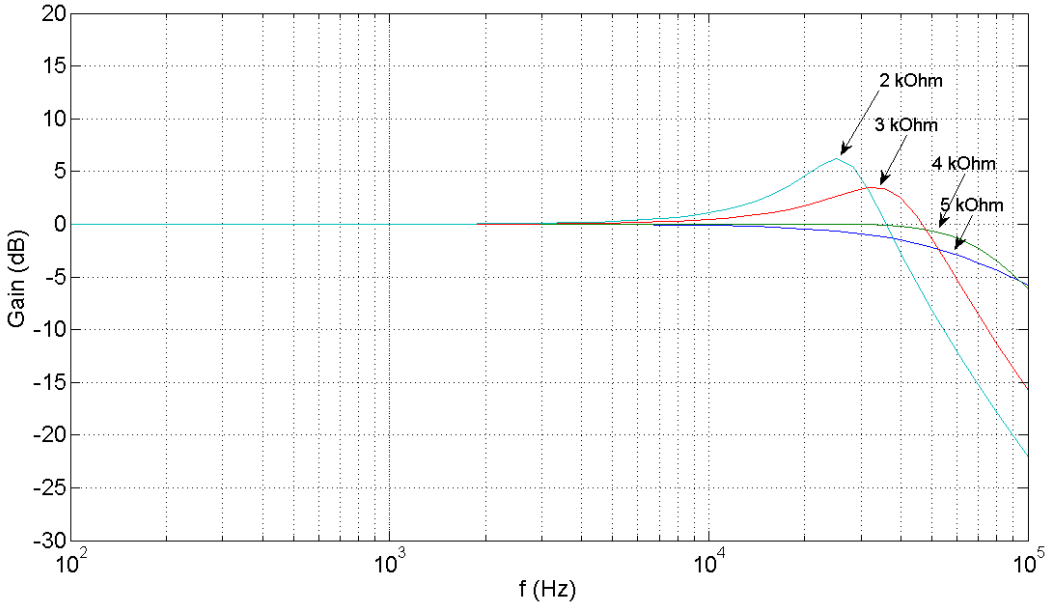

Figure 31. Simulated Frequency Response of Headstage Amplifier with TLE2037

Commercial resistors in the 1 GOhm range typically have a shunt capacitance in the order of 0.1pF [27] (Sigworth, 1995, p.97). It was assumed in the simulations that a parasitic capacitance of 8 fF exists across the 1GOhm feedback capacitance. The value of this capacitance affects the roll-off of the frequency response considerably. It was found that for values below 8 fF the roll-off disappears and response became unstable with a huge rise in the gain.

The simulated responses were compared with frequency response measurements on the fabricated headstage boards using the setup explained earlier. (Sec. 3.5, p.31) Figure. 32 – 35.

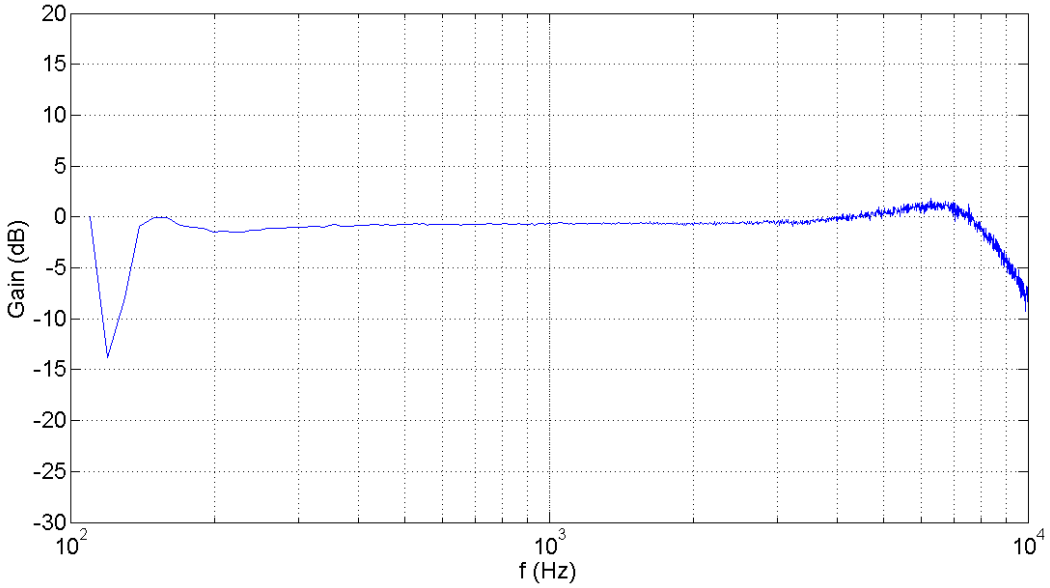

Figure 32. Measured Frequency Response of Headstage Amplifier with OPA 656

The measured frequency response of the Headstage amplifier with OPA 656 is flat up to 3 kHz, similar to the simulated response. However at the best noise performance setting, the circuit oscillates at frequencies above 4 kHz. The

increase in noise at high frequencies could be due to the reduced dynamic range of the Op amp because of lower operating voltage at 5 V. leading to lower signal to noise ratio.

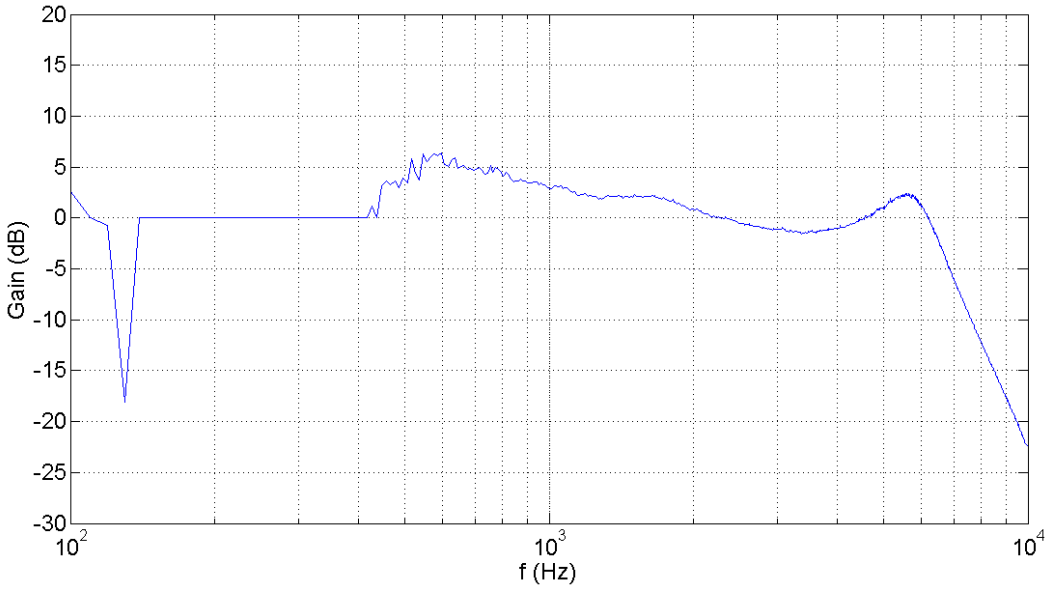

Figure 33. Measured frequency response of headstage with OPA 827

The measured frequency response of OPA 827 and OPA 134 are similar with bandwidths in the same order of 6 kHz. An oscillation is still observed near the roll-off point. However the response is not flat unlike that of the OPA 656. The roll-off, however is steep in both cases when compared to the OPA 656.

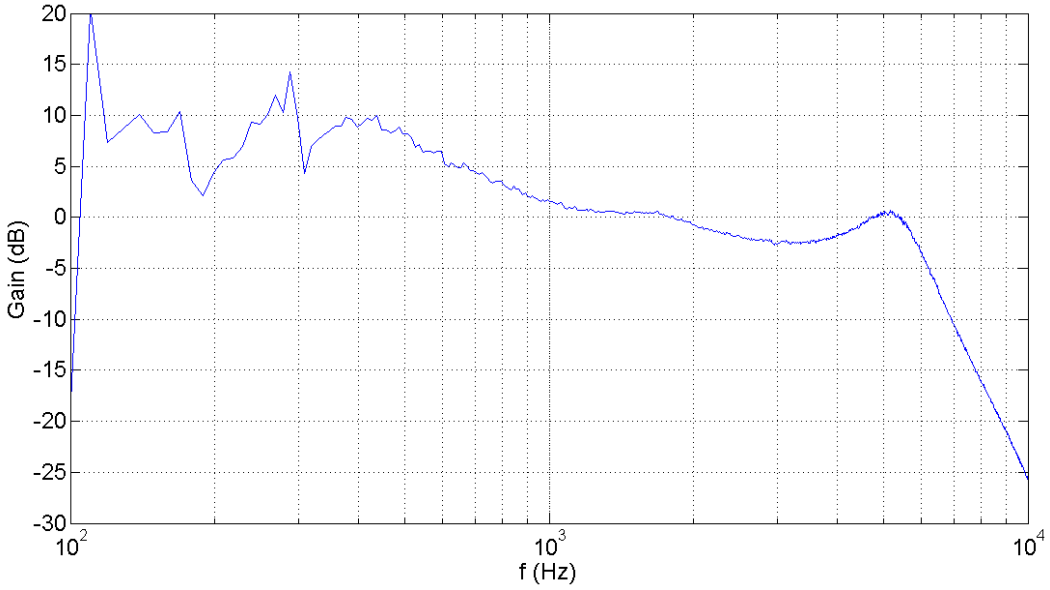

Figure 34. Measured frequency response of headstage with OPA 134

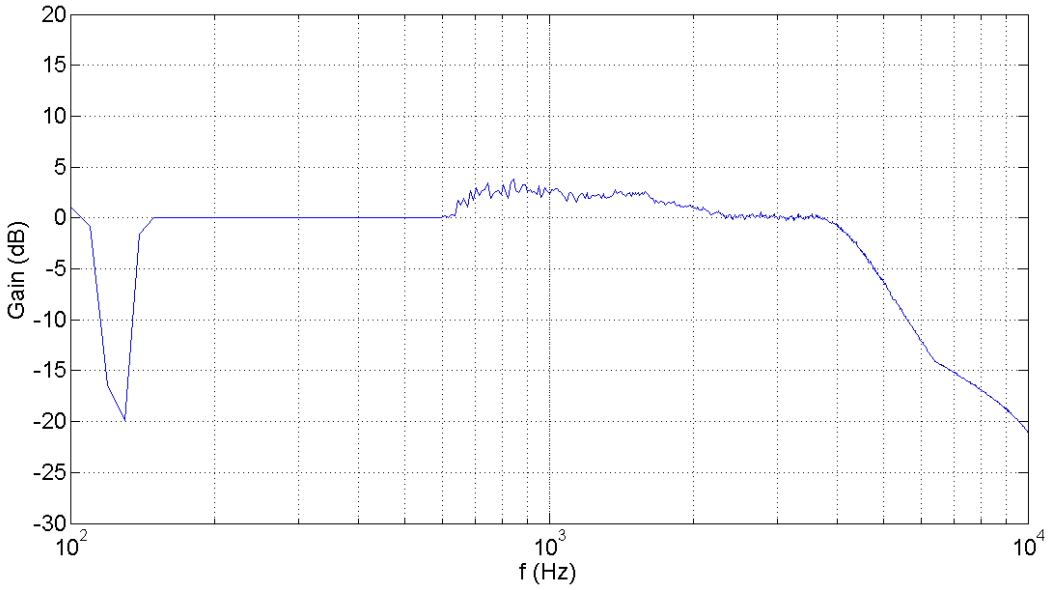

Figure 35. Measured frequency response of headstage with TLE2037

The TLE 2037 exhibits a flat response till frequencies up to 4 kHz. The roll off is steep when compared to the OPA 656, but shallower than that observed for the

OPA 134 and OPA 827. The roll-off also exhibits a second cut-off around 6 kHz. It is notable that the TLE 2037 does not oscillate at the best noise performance setting.

When comparing the results, it is also important to consider the setup, using which the Op-amps were mounted on to the headstage. The OPA 656 was soldered on to the headstage during measurements. However, all other three op-amps were mounted in a ZIF socket for ease of testing. This arrangement introduces considerable parasitic capacitances that have to be taken into account.

At lower frequencies of measurement, the lock-in amplifiers take a finite time to lock-in to the measured signal, thereby distorting the measured output voltage.

4.2.2 Noise analysis:

A noise analysis was also performed on the simulated circuit with all four Op-amps and the spectral density in A^2/Hz was plotted respectively. The spectral density was obtained for the same settings of JFET drain bias used to plot the frequency response. (Figures 36-39). The noise analysis performed using PSPICE indicates noise characteristics that are similar to the frequency response for the respective drain bias settings.

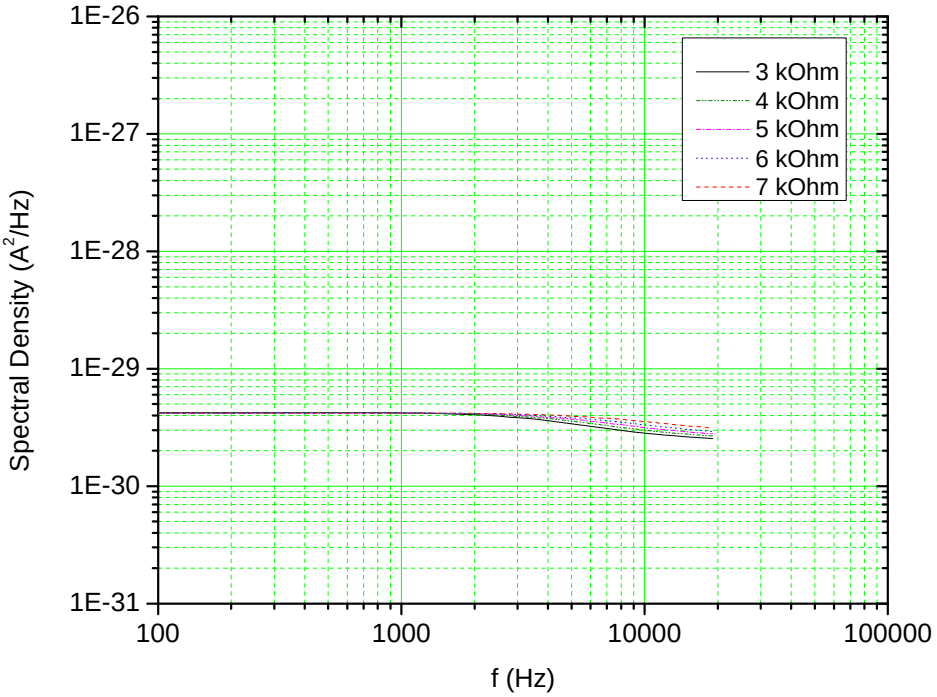

Figure 36. Simulated headstage output noise with OPA 656

The OPA 656 exhibits a flat spectral density of 4e-29 A^2/Hz up to 3 kHz after which it starts to roll-off. In case of OPA 827, the spectral density maintains a flat profile up to 5 kHz. However when the circuit oscillates, the noise level increases as seen. Similarly a flat response is seen for OPA 134 up to 6 kHz with an increase in noise level up to a maximum of 2e-28 A^2/Hz when the circuit oscillates.

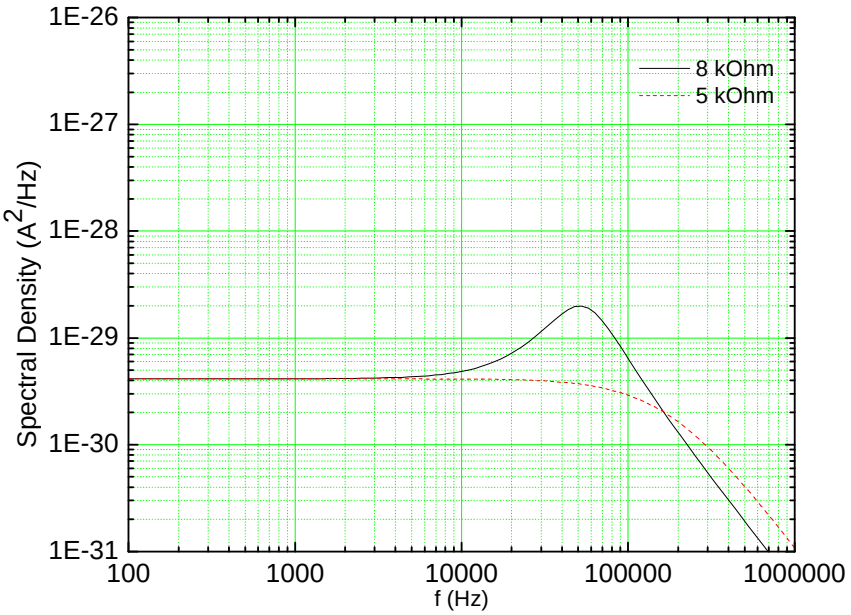

Figure 37. Simulated headstage output noise with OPA 827

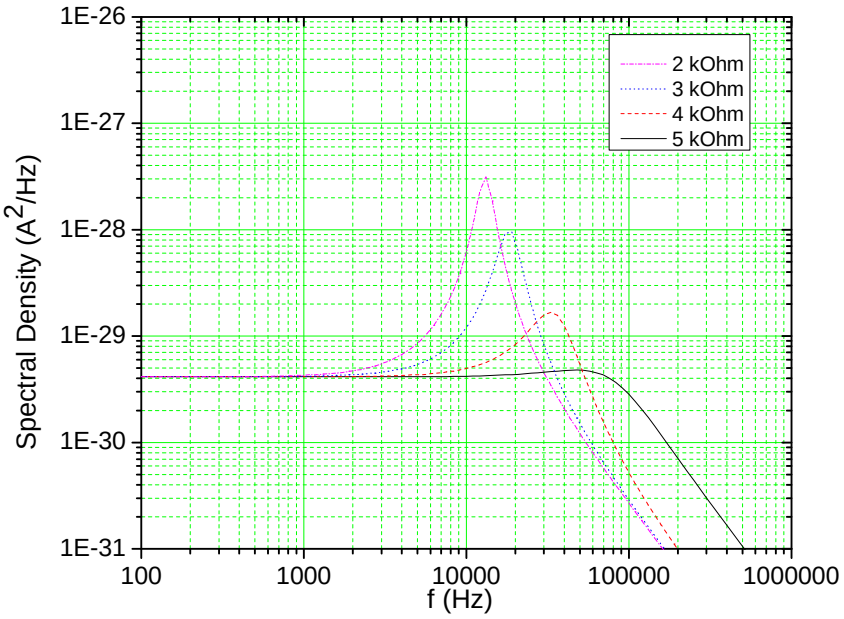

Figure 38. Simulated headstage output noise with OPA 134

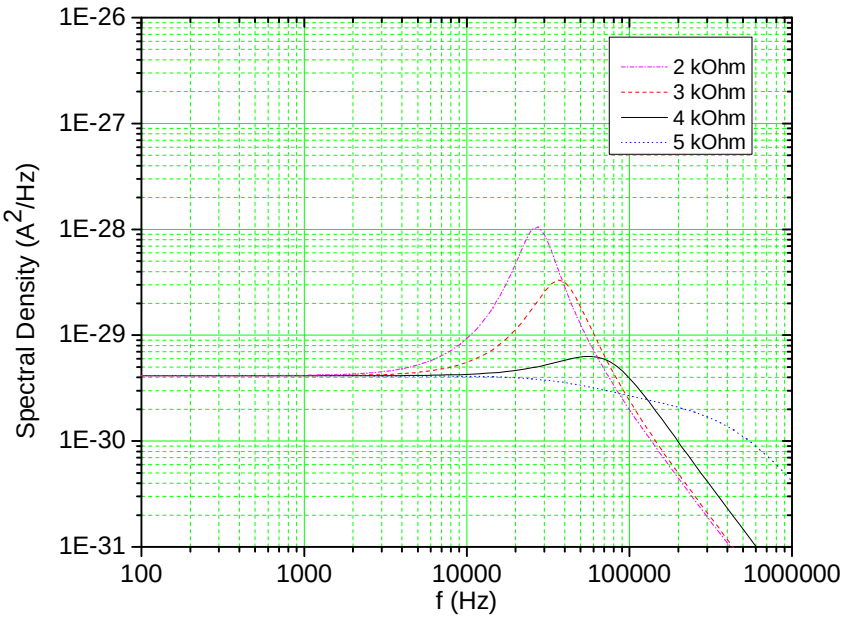

Figure 39. Simulated headstage output noise with TLE 2037

The headstage output was then connected to a HP 3562A Dynamic Signal Analyzer and the response was obtained with all four Op-amps listed in Table 1. (Figure 40 – 43). The measurement was done again with all four Op amps, with a 1GOhm load connected across the output of the amplifier. This was done in order to model the gigaseal formed by a lipid bilayer across which the ionic current is measured by the headstage amplifier. It is seen that in case of OPA 134, OPA 827 and TLE 2037 with the 1 GOhm, the spectral density reduces after 1 kHz in comparison to the open load condition. In all four cases a roll off in the noise level is seen starting in the 10^{-29} A^2/Hz range and rolling off after 19 kHz. The measured spectral densities are in the same range as those that were simulated.

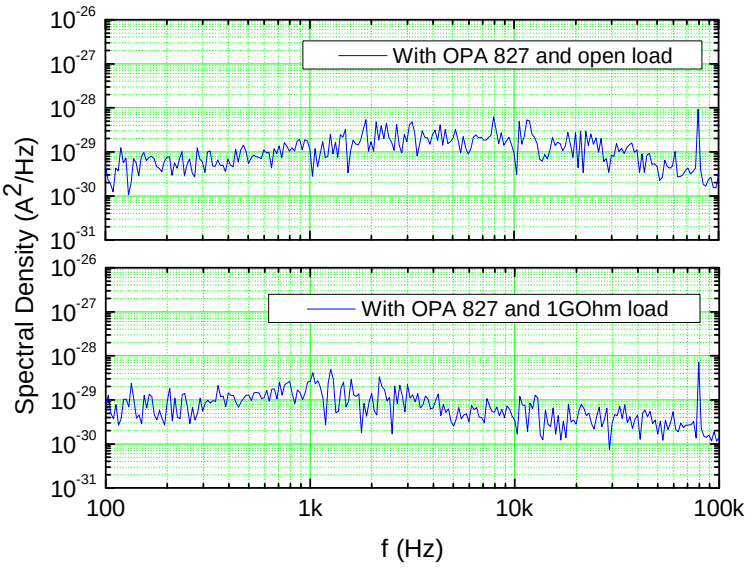

Figure 40. Spectral Density of headstage with OPA 827

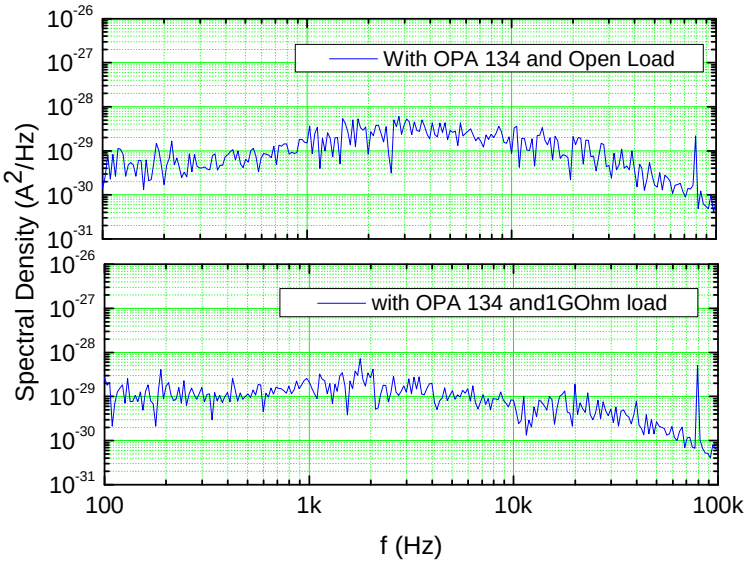

Figure 41. Spectral Density of Headstage with OPA 134

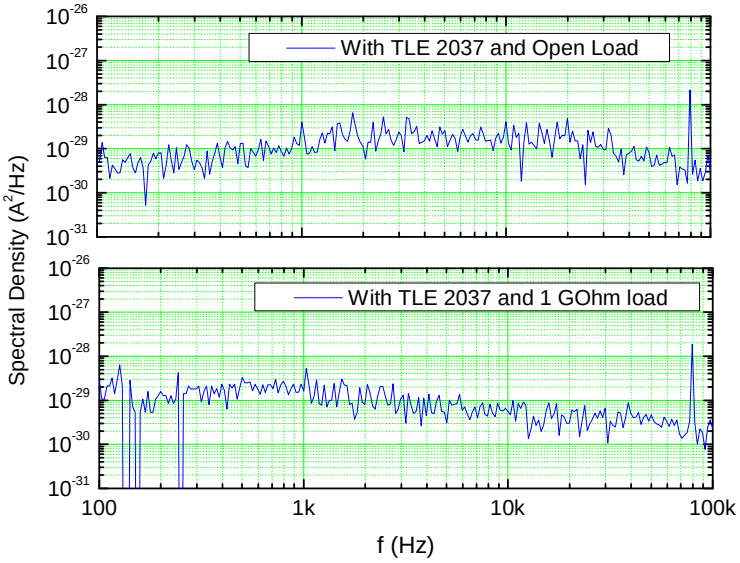

Figure 42. Spectral Density of headstage with TLE 2037

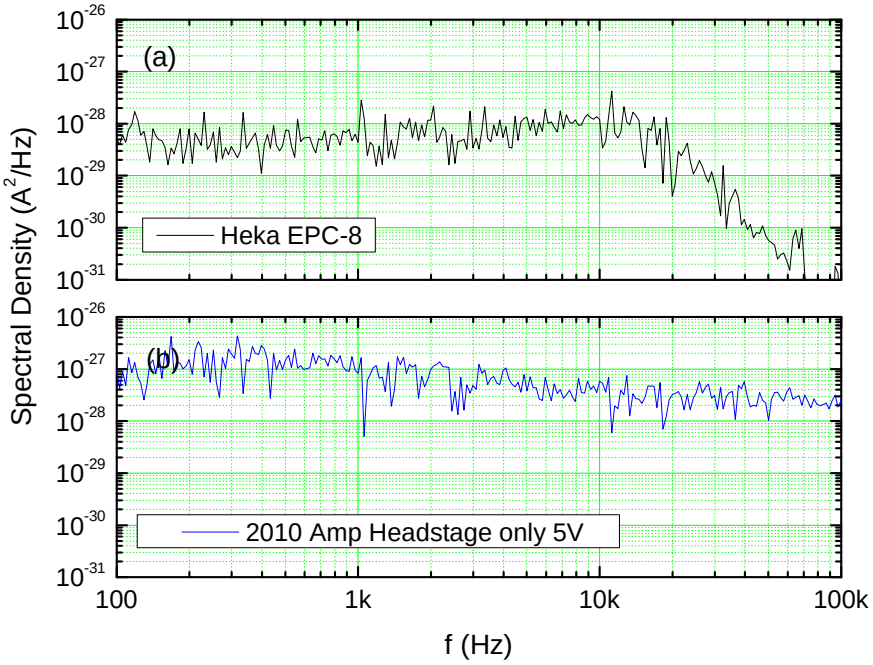

Figure 43. Spectral Density of headstage with OPA 656

In Figure 43, the spectral density of the Headstage amplifier with OPA 656 op amp and the HEKA EPC 8 is shown. The spectral density of the headstage designed with OPA 656 is higher than expected. This is because the ±12 V amplifier design [27] (Sigworth, 1995), is being operated at ± 5V. The reduced operating voltage has two implications on the noise levels. 1) Reduced operating voltage means reduction in the dynamic range of the circuit and reduction in signal to noise ratio. 2) The unmodified circuit is now operating at a lower supply voltage which shifts the JFET operating point. The operating point needs to be optimal for best noise performance and this optimization has to be done by re-designing the circuit with respect to the new supply voltage. The roll-off at 10 kHz can be achieved by connecting the control circuit at the output of the headstage.

4.3 Support Circuit board:

The support circuit was simulated and the frequency response was obtained without boost and with increasing values of the boost adjust resistor (Figure 44). The roll-off was maintained at 10 kHz. The input signal to the boost stage can be boosted by up to 10 dB in the 1 kHz to 10 kHz range. Thus, the corner frequency in the headstage can be replaced by a higher corner frequency by adjusting the frequency boost resistor. While maintaining the Frequency boost resistor at 30 kΩ the gain of the boost stage was varied and the response was plotted (Figure 45).

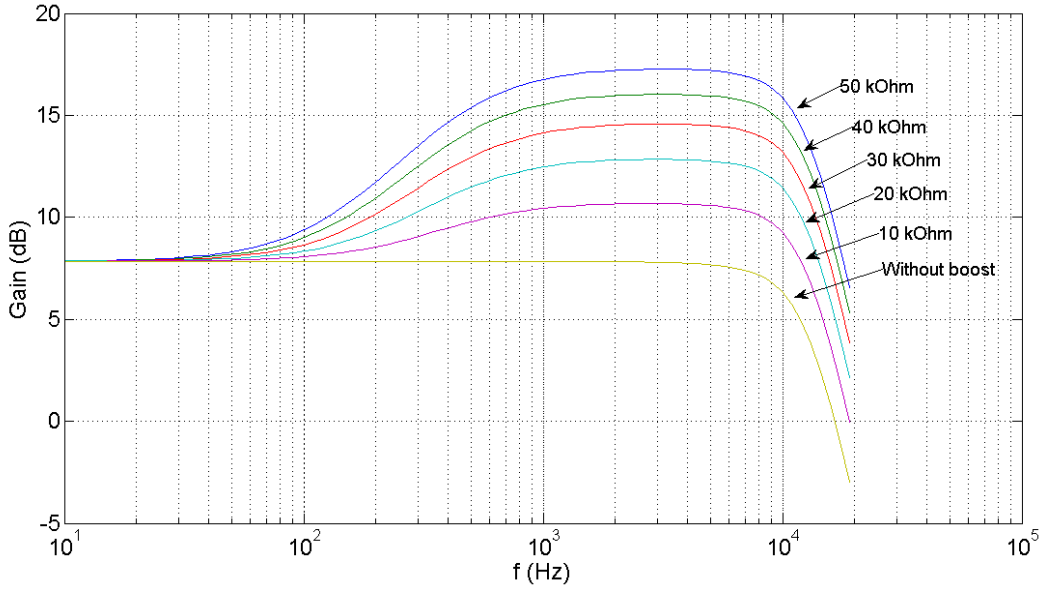

Figure 44. Frequency response of support circuit with frequency boost

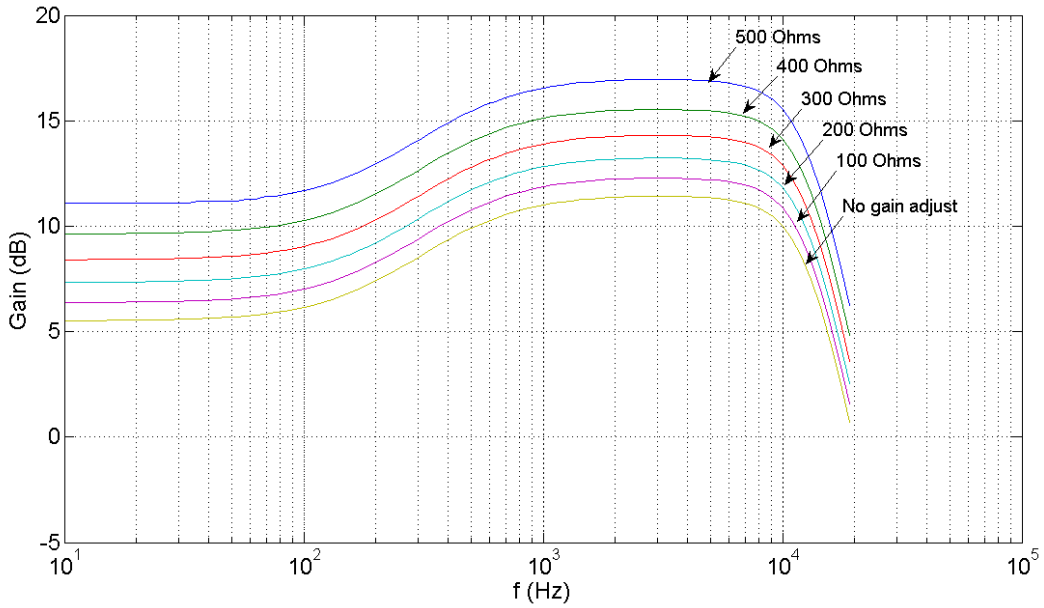

Figure 45. Frequency response of the boost circuit with variable gain

4.4 Switching of Ompf protein:

Bilayers were formed on all four micropores and OmpF was added to each well for self-insertion. The self-insertion of OmpF porin can be seen in Channel 2 of Figure 46.

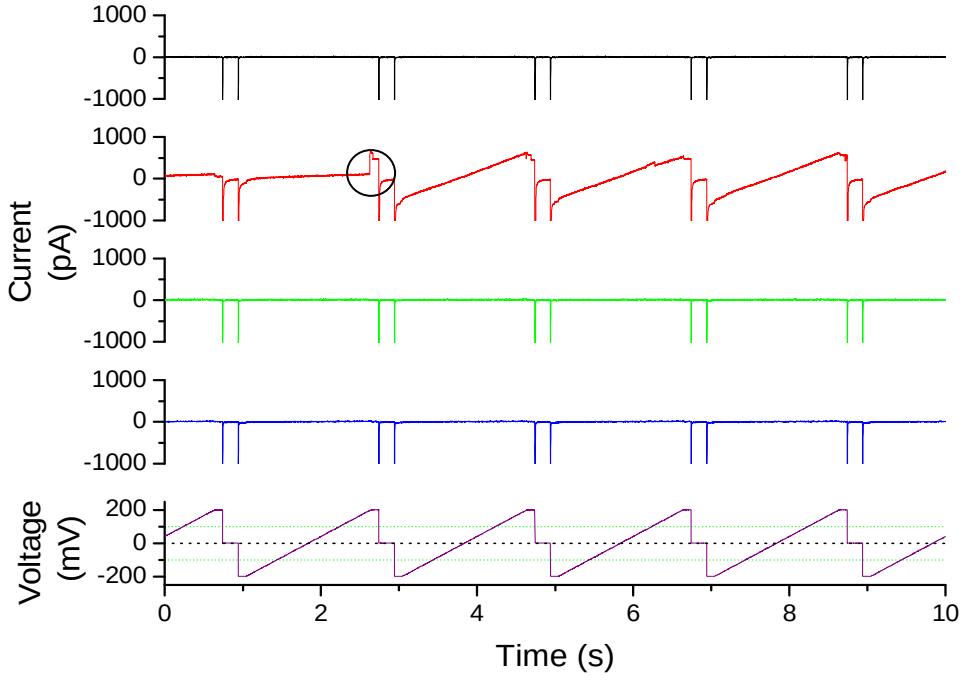

Figure 46. OmpF self insertion in 30 µm bilayer membrane in well 2

When self-insertion in a bilayer took place, the bilayers at the other three sites, stayed intact. It was also seen that "broken" bilayers or reforming the bilayers does not affect the bilayers at the neighbouring sites.

A simultaneous recording of OmpF gating at an apllied voltage of 200 mV can be seen in channel 2 and 3 in Figure 47. Observing the recorded events shows that, there is no crosstalk between the individual channels.

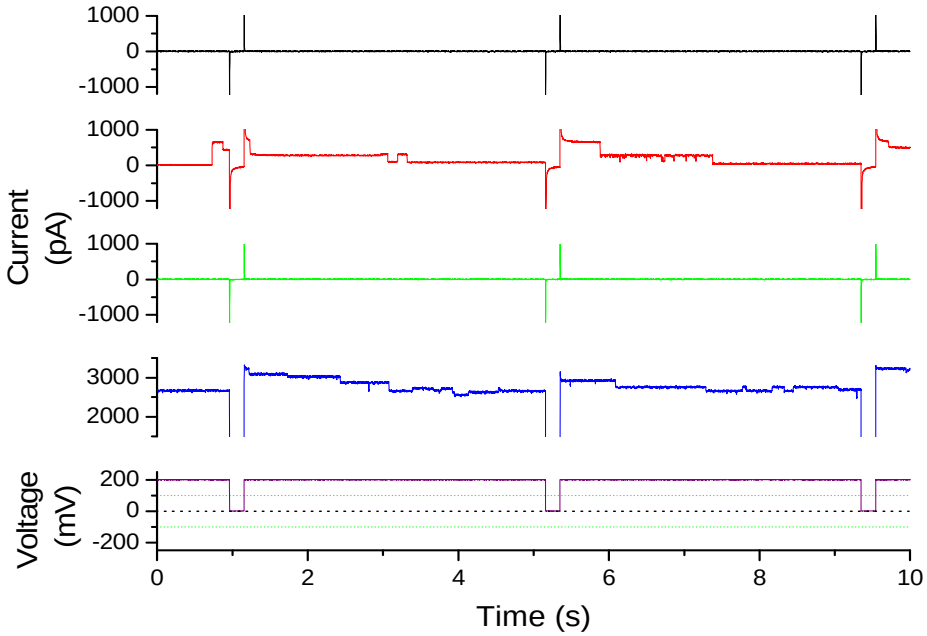

Figure 47. OmpF gating simultaneously in two separate membranes

The current-amplitude histogram of the OmpF gating currents was obtained (Figure 48) at 200 mV. The current varies from around 2000 pA to more than 2800 pA in steps which proves the increased gating activity of the trimer. The histogram plot shows that there are specific current levels at which the gating occurs.

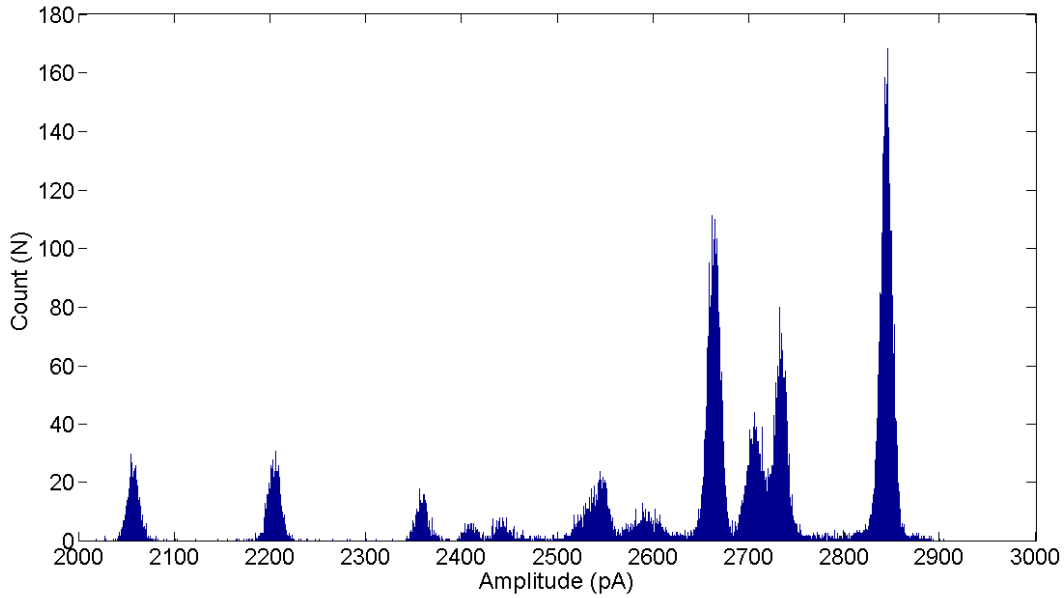

Figure 48. Current – Amplitude Histogram of OmpF gating.

The relative conductance steps, for the same recording is plotted in Figure 49 with the conductance at the lowest current as the reference. A number of sub conductance switching states with conductance less than monomeric conductance of, approximately 1.35 nS can be observed.

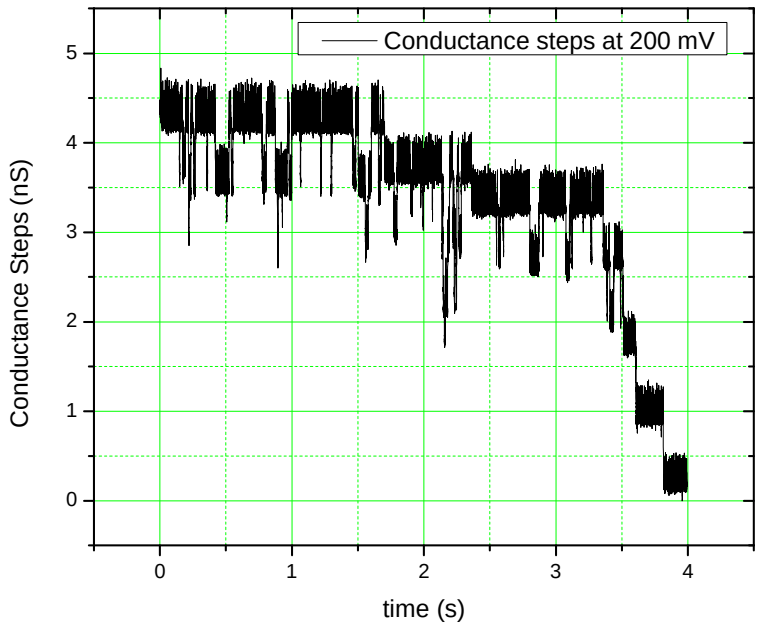

Figure 49. Conductance steps showing gating of the OmpF trimer

4.5 Switching of Ompf protein in the presence of Ampicillin:

Ampicillin (2.5 mM) was added to the second well and the effect of the antibiotic on the gating of OmpF was observed (Figure 50). In the figure, Channel 2 shows the effect of adding Ampicillin to a bilayer system with OmpF, channel 3 shows a bilayer system with no ampicillin added. The addition of ampicillin to well 2 does not affect the activity in the other wells. It can be seen that the current levels in the presence of Ampicillin are higher compared to the well not containing the antibiotic. This can be attributed to more than one trimeric porin channel being inserted in the open state.

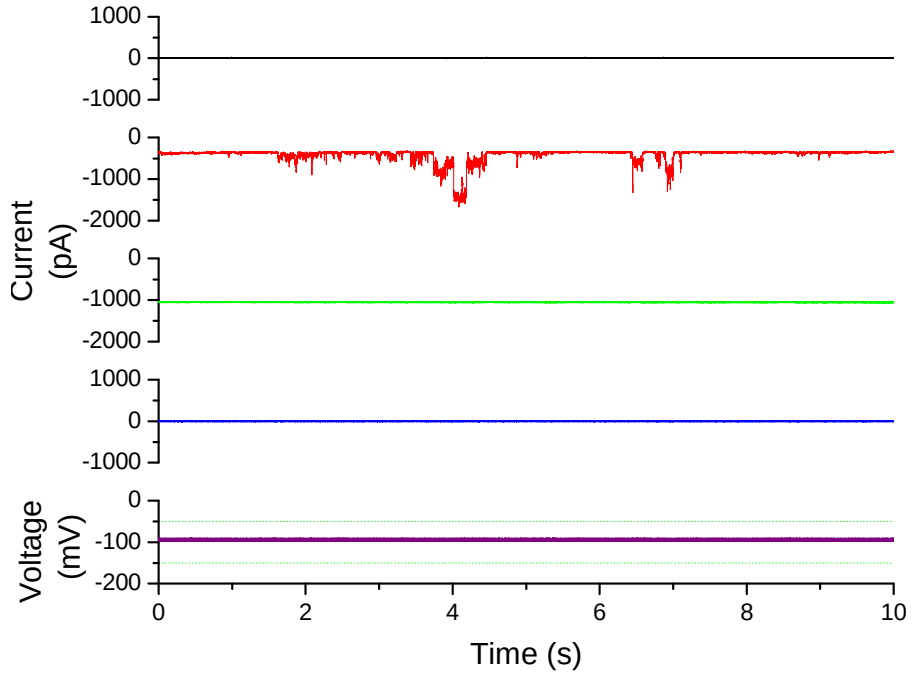

Figure 50. OmpF gating in two separate membranes with Ampicillin in well 2

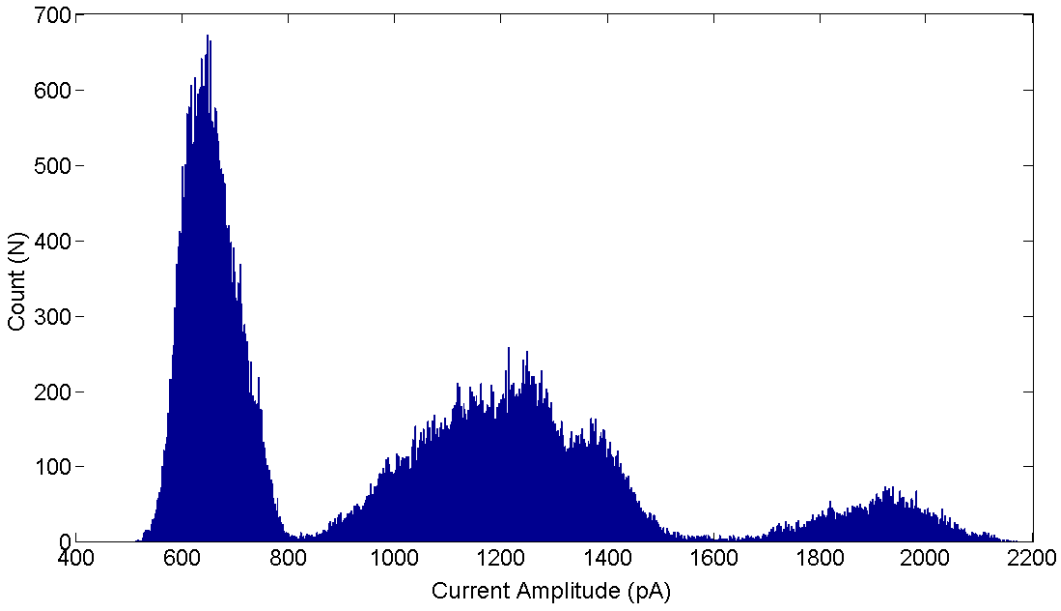

Figure 51. Current amplitude histogram of OmpF in the presence of ampicillin

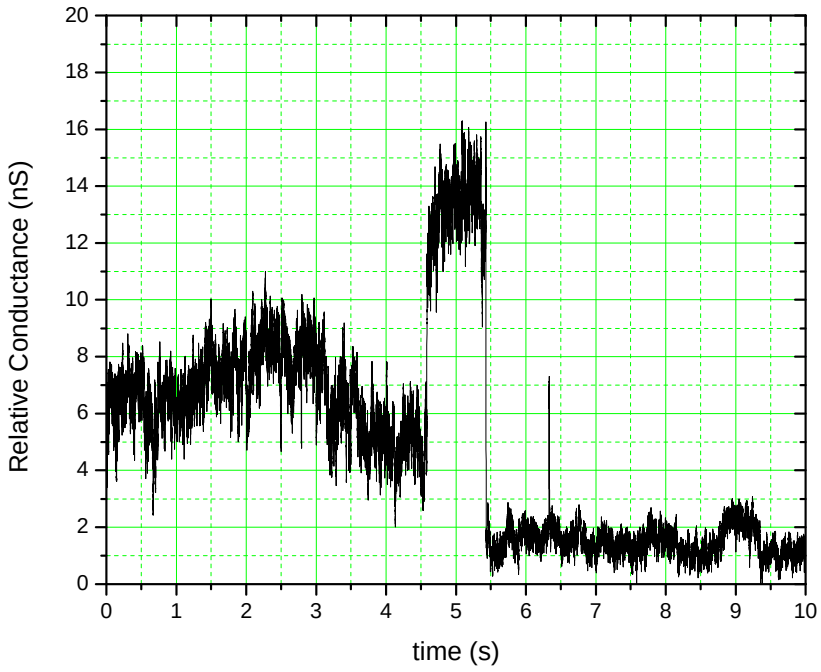

Figure 52. Conductance steps of OmpF gating in the presence of ampicillin

The relative conductance of the porin is shown in Figure 52 with reference to the conductance at lowest current measured. It can be seen that the conductance drops significantly after 4.5 s.

Since the Ampicillin molecule permeates through the open porin channel, it temporarily blocks part of the channel, leading to a reduction in open channel current. This causes a broad current amplitude distribution as seen in Fig. 51, contrary to the discrete conductance levels of the porin itself (cf. Fig. 48). This can be seen as a large variation of conductance steps in Figure 52.

Chapter 5

CONCLUSION

5.1 Conclusion

It has been demonstrated that stable lipid bilayers can be set up on an array of silicon micropores and can be used as sites for self-inserting ion-channel proteins which can be studied independently of each other. The 30 µm silicon pores used were vertically mounted in a fabricated acrylic holder with four wells and were painted with the lipid solution to form bilayers.

The need for simultaneous recording of currents in the four wells necessitated fabrication of inexpensive and small multi-channel headstage amplifiers. The frequency response and spectral density of the headstage was simulated and verified with measured frequency responses and spectral density. This was done with each of the four OPA and TLE Op amps from Table 1 to compare the performance of the circuit and to choose the best Op-amp for better noise response and Gain-Bandwidth product. The current design using an OPA656 op amp operating at ±5V and the discrete differential front end operating at ±12V was found to be an appropriate choice concerning noise and bandwidth. Alternatively, a design using a recently released high-voltage SiGe JFET Op-amp with a smaller gain bandwidth product (OPA827) can be used without affecting the noise performance or significant deterioration of the frequency response, but with the benefit of a larger dynamic range at ±12V supply voltage. Using

published designs, support circuits were constructed for the headstage to include a capacitance compensation circuit and a frequency boost circuit, including an anti-aliasing filter designed for a roll-off at 10 kHz.

The complete arrangement was then used to demonstrate the independence of individual channels from each other, during simultaneous measurement of lipid bilayer membrane gigaseals, of ionic current flow through OmpF porin ion channels and as a tool for studying ion channel permeation processes. To further show the independence of channels, the permeation process of antibiotics was studied. Ampicillin (2.5 mM) was added to one of the fluidic wells and the ionic currents in both wells were recorded again.

By analyzing the recorded currents, it can be clearly seen that the conductance steps of the current recorded from the well containing ampicillin and OmpF are larger compared to the well that contains only OmpF and that the frequency of events increases. The levels indicate that ampicillin permeates through the porin thereby temporarily reducing the conductance of the porin.

5.2 Future Work

It would be practical to make a six chamber array in order to create a set of chambers near the screw joints in case of cracks due to stress. In addition, the back side of the holder is proposed to be divided into identical channels to achieve

total isolation of the individual channels, allowing individual voltage stimulation protocols.

An OPA656 Op-amp design with ±5V power supply is proposed to be simulated and used in the next revision of the headstage circuit with scaled current and voltage values. Steps towards integrating more of the support circuit onto the headstage board can be taken. The capacitance compensation circuit, for instance, can be incorporated within the headstage. The headstage and control circuit together provide an inexpensive method of simultaneous recording from different bilayer sites.

The Montal Mueller method using the syringe pump can be used with microfluidics and horizontally mounted silicon micropores and integrated electrodes to achieve contactless bilayer formation. The multi channel configuration can be used to conduct experiments on different types of ion-channels with different sensitivities simultaneously.

REFERENCES

[1] Aboud, S., Marreiro1 D., Saraniti, M., Eisenberg, R. (2005). The role of long-range forces in Porin channel conduction, *Journal of Computational Electronics,* 4:175–178.

[2] Axopatch 200B manual and circuit diagram, http://www.moleculardevices.com/Products/Instruments/Conventional-Patch-Clamp/Axon-Axopatch.html

[3] Baaken, G., Sondermann, M., Schlemmer, C., Rühe, J., Behrends, J.C. (2008). Planar microelectrode-cavity array for high-resolution and parallel electrical recording of membrane ionic currents, *THE ROYAL SOCIETY OF CHEMISTRY, LAB CHIP, 2008, 8,* 938 - 944.

[4] Bayley, H., Cremer, P.S. Stochastic sensors inspired by biology, *NATURE, VOL 413,* 226 - 230.

[5] Castellana, E.T., Cramer, P.S. (2006). Solid supported lipid bilayers: From biophysical studies to sensor design, *SURFACE SCIENCE REPORTS, 61,* 429 - 444.

[6] Cremer, P.S., Yang,T. (1999). Creating Spatially Addressed Arrays of Planar Supported Fluid Phospholipid Membranes. *JOURNAL OF AMERICAN CHEMICAL SOCIETY, 121,* 8130 -8131

[7] Danelon, C., Nestorovich, E.M., Winterhalter, M., Ceccarelli, M., Bezrukov, (2006) S.M. Interaction of Zwitterionic Penicillins with the OmpF Channel Facilitates
Their Translocation, *BIOPHYSICAL JOURNAL, Vol.90,* 1617 - 1627.

[8] Gore, A., Chakrabartty, S., Pal, S., Alocilja, E.C. (2006). A Multichannel Femtoampere-Sensitivity Potentiostat Array for Biosensing Applications. *IEEE TRANSACTIONS ON CIRCUITS AND SYSTEMS—I: REGULAR PAPERS, VOL. 53, NO. 11, NOVEMBER 2006,* 2357 - 2363.

[9] Goryll, M., Chaplot, N. (2009). Miniaturized silicon apertures for lipid bilayer reconstitution experiments, *PROCEEDINGS OF MATERIALS RESEARCH SOCIETY, Vol.1191*.

[10] Guvench, M.G. (1994). SPICE Parameter Extraction From Automated Measurement Of JFET and MOSFET Characteristics In The Computer-Integrated Electronics Laboratory, *PROCEEDINGS OF A.S.E.E*

[11] Hamill, O.P., Marty, A., Neher, E., Sakmann, B., Sigworth, F.J. (1981). Improved Patch-Clamp Techniques for High-Resolution Current Recording from Cells and Cell-Free Membrane Patches. *PFLÜGERS ARCHIV (1981),* 391:85-100.

[12] Hamill, O.P., Sakmann B. (1980). A cell-free method for recording single-channel currents from biological membranes, *PROCEEDINGS OF PHYSIOLOGICAL SOCIETY, 1980,*41.

[13] HEKA EPC 7, EPC 8, EPC 8 plus patch clamp amplifier manual

[14] HEKA EPC 9 patch clamp amplifier manual, http://www.heka.com/download/manuals/epc9.pdf

[15] Kim, D., Koo, J. (2005). A low-noise and wide-band ac boosting current-to-voltage amplifier for scanning tunneling microscopy, *AMERICAN INSTITUTE OF PHYSICS*. DOI: 10.1063/1.1841873

[16] Kreir, M., Farre, C., Beckler, M., George, M., Fertig, N. (2008). Rapid screening of membrane protein activity: electrophysiological analysis of OmpF reconstituted in proteoliposomes, *THE ROYAL SOCIETY OF CHEMISTRY 2008, Lab Chip,* 587 - 595. DOI: 10.1039/b713982a

[17] Levis, R.A., Rae, J.L., (1984), Patch voltage clamp of lens epithelial cells: Theory and practice, *MOLECULAR PHYSIOLOGY, 6,* 115 - 162.

[18] Levis, R.A., Rae, J.L., (1993). The Use of Quartz Patch Pipettes for Low Noise Single Channel Recording. *BIOPHYSICAL JOURNAL, VOLUME 65*, 1666 - 1677

[19] Mahendran, K.R., Chimerel, C., Mach, T., Winterhalter,M. (2009) Antibiotic translocation through membrane channels: temperature-dependent ion current fluctuation for catching the fast events, *BIOPHYSICAL JOURNAL 2009,* 38:1141 - 1145. DOI 10.1007/s00249-009-0495-0

[20] Mayer, M., Kriebel,J.K., Tosteson, M.T., Whitesides, G.M. (2003). Microfabricated Teflon Membranes for Low-Noise Recordings of Ion Channels in Planar Lipid Bilayers, *BIOPHYSICAL JOURNAL, Vol.84*, 2684 - 2695.

[21] Miller, C. (1996). *Ion channel reconstitution*, New York: Plenum Press.

[22] Neher, E., Sakmann, B. (1976). Single channel currents recorded from membrane of denervated frog muscle fibres, *NATURE, Vol. 260,* 799 - 802.

[23] Niles, W.D., Levis, R.A., Cohen, F.S. (1988). Planar bilayer membranes made from phospholipid monolayers form by a thinning process, *BIOPHYSICAL JOURNAL, Vol.53,* 327 - 335.

[24] Osaki, T., Suzuki, H., Pioufle, B.L., Takeuchi, S. (2009). Multichannel Simultaneous Measurements of Single-Molecule Translocation in α-Hemolysin Nanopore Array. *ANALYTICAL CHEMISTRY, Vol. 81, No. 24,* 9866 - 9870.

[25] Pantoja, R., Nagarah, J.M., Starace, D.M., Melosh, N.A., Blunck, R., Bezanilla, F., Heath, J.R. (2004). Silicon chip-based patch-clamp electrodes integrated
with PDMS microfluidics, *BIOSENSORS AND BIOELECTRONICS, 20,* 509–517

[26] PHD2000 syringe pump series User's manual, Harvard apparatus

[27] Sakmann, B., Neher, E. (1995). *Single channel recording,* New York: Plenum Press.

[28] Sigworth, F.J. (1995). Design of the EPC-9, a computer-controlled patch-clamp amplifier. 1. Hardware. *JOURNAL OF NEUROSCIENCE METHOD,* 56: 195 - 20.

[29] Tartagni, M., Thei, F., Rossi, M., Bennati, M., Crescentini, M., Lodesani, F., Morgan, H. (2010). Parallel Recording of Single Ion Channels: A Heterogeneous System Approach. *IEEE TRANSACTIONS ON NANOTECHNOLOGY, VOL. 9, NO. 3, MAY 2010,* 295 - 302.

[30] Weerakoon, P., Klemic, K., Sigworth, F.J., Culurciello, E. (2008). A Low-Noise Miniaturized Patch-Clamp Amplifier, *IEEE/NIH LIFE SCIENCE SYSTEMS AND APPLICATIONS WORKSHOP (LISSA 2007,* 164 - 167

[31] Weerakoona, P., Culurciellob, E., Yangc, Y., Santos-Sacchic, J., Kindlmann, P.J., Sigworth, F.J. Patch-clamp amplifiers on a chip, *JOURNAL OF NEUROSCIENCE METHODS 192 (2010),* 187 - 192.

[32] Wilk, S., (2005), Dissertation on Microfabricated silicon apertures for transmembrane ion channel measurement, Arizona State University

[33] Yoshimura, F., Nikaido, H. (1985). Diffusion of β-Lactam Antibiotics through the Porin Channels of Escherichia coli K-12. *ANTIMICROBIAL AGENTS AND CHEMOTHERAPY, Jan. 1985, Vol.27, No.1*, 84-92.

[34] Zhao, Q., Wang, D., Jayawardhana, D.A, Guan, X. (2008). Stochastic sensing of biomolecules in a nanopore sensor.